Lung group 2 innate lymphoid cells differentially depend on local IL-7 for their distribution, activation, and maintenance in innate and adaptive immunity-mediated airway inflammation

Daichi Takami[1,2], Shinya Abe[1], Akihiro Shimba[1,3], Takuma Asahi[1,4], Guangwei Cui[1], Shizue Tani-ichi[1,3], Takahiro Hara[1], Keishi Miyata[5], Masashi Ikutani[6], Kiyoshi Takatsu[7], Yuichi Oike[5], and Koichi Ikuta[1,*]

[1]Laboratory of Immune Regulation, Department of Virus Research, Institute for Life and Medical Sciences, Kyoto University, Kyoto 606-8507, Japan; [2]Graduate School of Pharmaceutical Sciences, Kyoto University, Kyoto 606-8501, Japan, [3]Department of Human Health Sciences, Graduate School of Medicine, Kyoto University, Kyoto 606-8507, Japan, [4]Graduate School of Medicine, Kyoto University, Kyoto 606-8501, Japan, [5]Department of Molecular Genetics, Graduate School of Medical Sciences, Kumamoto University, Kumamoto 860-8556, Japan; [6]Graduate School of Integrated Sciences for Life, Hiroshima University, Higashi-Hiroshima 739-8511, Japan; and [7]Toyama Prefectural Institute for Pharmaceutical Research, Toyama 930-8501, Japan.

[*]Correspondence:
E-mail address: ikuta.koichi.6c@kyoto-u.ac.jp
Laboratory of Immune Regulation, Department of Virus Research, Institute for Life and Medical Sciences, Kyoto University, Kyoto 606-8507, Japan
Tel, +81-75-751-4012; Fax, +81-75-751-4810.

Running title: Local IL-7 controls lung ILC2s in inflammation

Keywords: ILC2, Th2 cell, IL-5, bronchoalveolar epithelial cell, lymphatic endothelial cell

Number of pages: 34
Number of figures: 7
Number of supplementary figures: 11

Abstract

IL-7 is a cytokine critical for the development and maintenance of group 2 innate lymphoid cells (ILC2s). ILC2s are resident in peripheral tissues such as the intestine and lung. However, whether IL-7 produced in the lung plays a role in the maintenance and function of lung ILC2s during airway inflammation remains unknown. IL-7 was expressed in bronchoalveolar epithelial cells and lymphatic endothelial cells (LECs). To investigate the role of local IL-7 in lung ILC2s, we generated two types of IL-7 conditional knockout (IL-7cKO) mice: Sftpc-Cre (SPC-Cre) IL-7cKO mice specific for bronchial epithelial cells and type 2 alveolar epithelial cells and Lyve1-Cre IL-7cKO mice specific for LECs. In steady state, ILC2s were located near airway epithelia, although lung ILC2s were unchanged in the two lines of IL-7cKO mice. In papain-induced airway inflammation dependent on innate immunity, lung ILC2s localized near bronchia via CCR4 expression, and eosinophil infiltration and type 2 cytokine production were reduced in SPC-Cre IL-7cKO mice. In contrast, in house dust mite (HDM)-induced airway inflammation dependent on adaptive immunity, lung ILC2s localized near lymphatic vessels via their CCR2 expression two weeks after the last challenge. Furthermore, lung ILC2s were decreased in Lyve1-Cre IL-7cKO mice in the HDM-induced inflammation due to decreased cell survival and proliferation. Finally, administration of anti-IL-7 antibody attenuated papain-induced inflammation by suppressing the activation of ILC2s. Thus, this study demonstrates that IL-7 produced by bronchoalveolar epithelial cells and LECs differentially controls the activation and maintenance of lung ILC2s, where they are localized in airway inflammation.

Introduction

Interleukin-7 (IL-7) is a cytokine essential for the development and homeostasis of T cells, B cells, and innate lymphoid cells (ILCs). IL-7 promotes the early development of B and T cells in the bone marrow and thymus (1, 2) and the homeostasis of naive and memory T cells in peripheral lymphoid organs (3, 4). These lymphocytes are drastically reduced in IL-7- and IL-7R-deficient mice (5, 6). IL-7-binding to the IL-7R activates the tyrosine kinases JAK1 and JAK3, which then phosphorylate and activate STAT5 and PI3K (7, 8). These molecules transduce the signals for cell proliferation, survival, and differentiation of lymphocytes (7). In lymphoid organs, IL-7 is produced by stromal cells such as bone marrow mesenchymal stromal cells, thymic epithelial cells, lymphatic endothelial cells (LECs), and fibroblastic reticular cells (9). In addition, in the periphery, IL-7 is produced by LECs in the skin and by LECs and epithelial cells in the gut (9). In the lung, IL-7 is produced by LECs, which support the maintenance of resident memory Th2 cells in allergic airway inflammation (10). However, whether stromal cells other than LECs produce IL-7 in the lung remains unknown.

Group 2 ILCs (ILC2s) produce type 2 cytokines in response to tissue damage in asthma, atopic dermatitis, and helminth infections (11). ILC2s are activated by cytokines, such as IL-33, IL-25, and thymic stromal lymphopoietin (TSLP), secreted by damaged epithelial cells (12-14). Upon stimulation, ILC2s rapidly produce IL-5, IL-13, IL-4, IL-9, and amphiregulin, which induce eosinophil chemotaxis, goblet cell metaplasia, IgE production, and tissue remodeling (15). ILC2s are tissue-resident and are found in peripheral tissues, such as the lung, skin, intestine, and adipose tissue (11, 15). In the lung, ILC2s are localized in the vicinity of bronchia, lymphatic vessels, and arteries in steady state, and adventitial stromal cells control the localization and function of ILC2s via TSLP and IL-33 (16-18). In addition, ILC2s increase in perivascular and peribronchial regions during airway inflammation (19, 20). ILC2s express some chemokine receptors, such as CCR4 and CCR8 (21). In asthmatic conditions, airway epithelial cells produce high levels of CCL17, a ligand of CCR4, and $CCR4^{+}IL\text{-}4^{+}$ Th2 cells localize near airway epithelia (22). Interaction of CCL1 or CCL8 with CCR8 expressed on ILC2s induces the localization of ILC2s near airway epithelia and Th2 cells (20, 23). In addition to ILC2s, resident memory Th2 cells in the lung also receive the signal of LEC-derived IL-7, resulting in their specific localization and function (10). Thus, local cytokines produced by stromal cells appear to control the distribution and function of tissue-resident immune cells. Although the localization of lung ILC2s in airway inflammation has been reported, whether the localization of lung ILC2s changes between steady state and different types of airway inflammation has not been investigated in detail.

ILC2s require IL-7 for development in vivo (24-26) and for maintenance and activation in vitro (24, 26-28). Since ILC2s are diminished in IL-7- and IL-7Rα-deficient mice (24), IL-7 is required for the development or maintenance of ILC2s. ILC2s differentiate from common lymphoid progenitors (CLPs), in which IL-7 induces the expression of nuclear factor IL-3-regulated protein (NFIL-3), the transcription factor required for ILC2 differentiation (26, 29). In addition, IL-7 is required for the survival and proliferation of ILC2s in culture (24). Since ILC2s are tissue-resident, the microenvironment and its local cytokines may be required for the maintenance and function of ILC2s. However, it remains unknown whether local IL-7 plays a role in the distribution and function of lung ILC2s.

To address these questions, we investigated the local function of IL-7 in the distribution, activation, and maintenance of lung ILC2s in two types of airway inflammation. We found that ILC2s are located close to airway epithelia in steady state and during papain-induced airway inflammation dependent on innate immunity. In contrast, they are located near lymphatic vessels in house dust mite (HDM)-induced airway inflammation, which is dependent on adaptive immunity. Using conditional knockout of IL-7 (IL-7cKO) in lung stromal cells, we

found that IL-7 produced by bronchoalveolar epithelial cells promotes ILC2 activation in papain-induced airway inflammation, whereas LEC-derived IL-7 maintains lung ILC2s in HDM-induced airway inflammation. Furthermore, administering an anti-IL-7 antibody attenuated papain-induced airway inflammation by suppressing ILC2 activation. Collectively, this study demonstrates that IL-7 produced by various stromal cells in the lung controls the distribution, activation, and maintenance of lung ILC2s, suggesting that the stromal microenvironment is an essential regulator of tissue-resident immune cells.

Materials and Methods

Mice

C57BL/6 mice were obtained from Japan SLC (Hamamatsu, Japan). Eight to twelve weeks old mice on a C57BL/6 background were analyzed. IL-7$^{GFP/+}$ mice (9) and IL-7$^{flox/flox}$ (30) mice were generated in our laboratory. IL-5$^{Venus/+}$ knock-in mice (31) were obtained from Riken BRC (Tsukuba, Japan). Sftpc-Cre (SPC-Cre) mice (32) and Lyve1-Cre mice (33) were obtained from Dr. Yuichi Oike at Kumamoto University and Dr. Jason Cyster at the University of California San Francisco, respectively. All mice were maintained under specific pathogen-free conditions in the Experimental Research Center for Infectious Diseases, the Institute for Life and Medical Sciences, Kyoto University. All mouse experiments were approved by the Animal Experimentation Committee of the Institute for Life and Medical Sciences, Kyoto University.

Antibodies and flow cytometry

The following fluorescent dye- or biotin-conjugated Abs were used: anti-CD3ε (145-2C11), CD4 (RM4-5), CD8α (53-6.7), NK1.1 (PK136), CD11b (M1/70), CD11c (N418), Gr-1 (RB6-8C5), CD45 (30-F11), Ter119 (Ter119), CD19 (6D5), B220 (RA3-6B2), CD5 (53-7.3), FcεRI (MAR-1), CD25 (PC61), KLRG1 (2F1/KLRG1), Sca-1 (E13-161.7), CD127 (IL-7R) (A7R34), ST2 (RMST2-2), GFP, EpCAM (G8.8), CD31 (MEC13.3), F4/80 (BM8), Siglec-F (E50-2440), MHC I-A/I-E (M5/114.15.2), gp38 (podoplanin) (8.1.1), CD69 (H1.2F3), CD103 (2E7), TCRβ (H57-597), CCR2 (475301), CCR4 (2G12), CD44 (IM7), IL-5 (TRFK5), IL-13 (eBio13A), Bcl-2 (BCL/10C4), and Ki-67 (SolA15). Fluorescent dye- or biotin-conjugated antibodies were purchased from BioLegend, eBioscience, and Invitrogen. PBS57-loaded CD1d tetramer was provided by the NIH Tetramer Core Facility. Biotinylated monoclonal antibodies were detected with Brilliant Violet 421 or 510-conjugated streptavidin (BioLegend). For Bcl-2 and Ki-67 staining, cells were fixed and permeabilized with the Foxp3/Transcription Factor Staining Buffer Set (eBioscience). For staining of IL-5 and IL-13, ILC2s were fixed and permeabilized with Intracellular Fixation and Permeabilization Buffer Set (eBioscience). Viable cells were analyzed on a BD LSRFortessa flow cytometer (BD Biosciences) using FlowJo software (BD Biosciences). In the figures, values in quadrants, gated areas, and interval gates indicate percentages in each population.

Cell preparation

After perfusion with phosphate-buffered saline (PBS), lungs were minced with scissors and incubated for 45 min at 37°C in 1.5 ml RPMI-1640 medium containing 10% fetal bovine serum, 1 mg/ml collagenase D (Roche Diagnostics) and 50 μg/ml DNase I (Worthington Biochemical). The digested lung fragments were passed through a 40-μm strainer. Leukocytes were separated by centrifugation through 30% Percoll. After erythrocyte lysis, cells were analyzed by flow cytometry. Bronchoalveolar lavage fluid (BALF) was obtained by infusion of 1 ml PBS through a catheter. For RNA-seq analysis and cell culture, ILC2s (Lineage$^-$IL-7R$^+$CD25$^+$Sca-1$^+$) were sorted from the lung using a FACS Aria III cell sorter (BD Biosciences). Lineage markers included CD3ε, CD4, CD8α, CD11b, CD11c, CD19, Gr-1, B220, CD5, FcεRI, CD45, and Ter119.

Cell culture

Sorted ILC2s (Lineage$^-$IL-7R$^+$CD25$^+$Sca-1$^+$, 5 × 10^3/well) were cultured on 96-well round-bottom plates in RPMI 1640 medium containing 10% fetal bovine serum, 50 μM 2-mercaptoethanol, 100 U/ml penicillin, and 100 μg/ml streptomycin with or without a cytokine cocktail for three days. The cocktail included IL-7 (10 ng/ml), IL-33 (10 ng/ml), or IL-2 (10 ng/ml).

Immunofluorescence staining
Freshly harvested lungs were fixed in 4% paraformaldehyde for 6 hours at 4℃ and replaced with a solution of 10, 20, and 30% sucrose in PBS at 4°C for 3 days. The tissues were embedded in O.C.T. compound (Sakura Finetechnical, Tokyo, Japan) and sliced at 30 μm thickness using a cryostat (Leica CM3050 S, Wetzlar, Germany). Fixed specimens were stained with DAPI, PE-EpCAM (G8.8), PE-NKp46 (29A1.4), Alexa Fluor 488-Lyve1 (ALY7), Brilliant Violet 421-CD3ε (145-2C11), anti-CD25 goat IgG, followed by Alexa Fluor 647 anti-goat IgG, and anti-GFP rabbit IgG, followed by Dylight649 anti-rabbit IgG, mounted with PermaFluor Aqueous Mounting Medium (Thermo Fisher Scientific, Waltham, MA, USA), and examined with a confocal laser scanning microscope (Leica TCS SP8). Antibodies were purchased from BioLegend and Invitrogen.

Image analysis
Images were analyzed using Imaris Bitplane 7.6 (Zeiss). ILC2s were identified by Venus expression in IL-5$^{Venus/+}$ mice. Three channels were generated to represent different structures: airways (EpCAM^{+}), lymphatics (Lyve1^{+}), and T cells (CD3^{+}). To calculate the distance between ILC2s and stromal cells, voxel-based surfaces of each expression in these images were rendered by a tool in Imaris. The shortest distance was measured between ILC2s and airways, ILC2s and lymphatics, and ILC2s and T cells. Image analysis was performed at the Medical Research Support Center, Graduate School of Medicine, Kyoto University, supported by the Platform for Drug Discovery, Informatics, and Structural Life Science of the Ministry of Education, Culture, Sports, Science and Technology, Japan.

Histology
Lungs were dissected after perfusion with 50 ml of PBS. Tissues were fixed in 4% paraformaldehyde for 12 hours at 4°C and replaced with a solution of 10, 20, and 30% sucrose in PBS at 4°C for 3 days. Sections of 10 μm thickness were stained with hematoxin and eosin (H&E).

Airway inflammation
Innate immunity-mediated airway inflammation was induced by treating 8- to 12-week-old mice with 100 μg papain (Sigma) in 50 μl of PBS intranasally (i.n.) on days 0, 1, and 2. Mice were sacrificed on day 3, and lungs and BALF were collected. Some lung sections were fixed in 4% formaldehyde. Adaptive immunity-mediated airway inflammation was induced by house dust mite (HDM, ITEA Inc.). Mice were sensitized intraperitoneally (i.p.) with 10 μg HDM emulsified in Imject Alum (Thermo Scientific) on day 0 and day 14. On days 21, 22, and 23, the mice were challenged i.n. with 10 μg HDM in 50 μl of PBS. Mice were sacrificed on day 37, and lungs and BALF were collected. Some lung sections were fixed in 4% formaldehyde.

Administration of anti-IL-7 antibody in vivo
Human anti-mouse/human IL-7 antibody (M25, Bio X Cell) and isotype-matched control antibody (IgG2b, Bio X Cell) were used for the IL-7 blocking experiment. For each experiment, wild-type mice were treated with 500 μg/mouse blocking antibody or isotype-matched control antibody. Wild-type (WT) mice were treated intraperitoneally with 500 μg/mouse anti-IL-7 monoclonal antibody or isotype control (day 0), administrated i.n. with papain at 3 hours and on days 1 and 2, and analyzed on day 3.

Administration of anti-CCL2 antibody in vivo
Armenian hamster anti-mouse/human/rat CCL2 antibody (2H5, Bio X Cell) and isotype-

matched control polyclonal antibody (IgG, Bio X Cell) were used for the CCL2 blocking experiment. For each experiment, wild-type mice were given i.p. with HDM emulsified in Imject Alum on day 0 and day 14. On day 21, the mice were treated with 200 μg/mouse anti-CCL17 antibody or isotype control, administered with HDM after 3 hours and on days 22 and 23, and analyzed on day 37.

Administration of anti-CCL17 antibody in vivo
Goat anti-mouse CCL17 polyclonal antibody (R & D Systems) and isotype-matched control antibody (IgG, R & D Systems) were used for the CCL17 blocking experiment. For each experiment, WT mice were treated i.n. with 20 μg/mouse anti-CCL17 antibody or isotype control (day 0), administered i.n. with papain after 3 hours and on days 1 and 2 and analyzed on day 3.

ELISA
The concentrations of IL-5 and IL-13 in BALF and culture supernatants were assessed using the IL-5 mouse uncoated ELISA kit (Invitrogen) and the IL-13 mouse uncoated ELISA kit (Invitrogen), respectively.

RT-PCR
Total RNA was extracted with Sepasol-RNA I Super G reagent (Nacalai Tesque) and treated with citrate buffer-saturated phenol (Nacalai Tesque). After genomic DNA was digested with DNase I, RNA was reverse transcribed using ReverTra Ace (Toyobo) with the random primer (Invitrogen) for ILC2s or the oligo(dT)$_{12\text{-}18}$ primer (Thermo Fisher) for lung stromal cells. cDNA from ILC2s was amplified in triplicate using TB Green Premix ExTaqII (Takara) with ROX reference dye (Takara) on a StepOnePlus real-time PCR system (Thermo Fisher Scientific). PCR was performed at 95°C for 30 sec, followed by 45 cycles of 95°C for 5 sec and 60°C for 30 sec. cDNA from stromal cells was amplified in duplicate using QuantiTect SYBR Green PCR Master Mix (Qiagen) with ROX reference dye (Invitrogen) on a StepOne Plus real-time PCR system. PCR was performed at 95°C for 15 sec, 55°C for 30 sec, and 72°C for 60 sec. cDNA from whole lung cells of wild-type mice was used as an amplification standard. Transcript levels were normalized to hypoxanthine-guanine phosphoribosyltransferase (HPRT) mRNA. Primer sequences are as follows: IL-7, 5'-TCCTCCACTGATCCTTGTTC-3' and 5'-CTTCAACTTGCGAGCAGCAC-3'; CCR2, 5'-GATTCACCACATGTGCTAAG-3' and 5'-CGTAGTCATACGGTGTGGTG-3'; CCR4, 5'-GGAAGGTATCAAGGCATTTGGG-3' and 5'-GTACACGTCCGTCATGGACTT-3'; CCR7, 5'-TCATTGCCGTGGTGGTAGTCTTCA-3' and 5'-ATGTTGAGCTGCTTGCTGGTTTCG-3'; HPRT, 5'-GTTGGATACAGGCCAGACTTTGTTG-3' and 5'-GATTCAACTTGCGCTCATCTTAGGC-3' ; IL-33, 5'-GAGCATCCAAGGAACTTCAC -3' and 5'-TAGTAGCACCTGGTCTTGC -3'.

RNA-seq analysis
Sorted ILC2s were lysed with buffer LTR (Qiagen) and purified with RNAClean XP (Beckman Coulter). Double-stranded cDNA was synthesized using the SMART-Seq v4 Ultra Low Input RNA kit for Sequencing (Takara), and sequencing libraries were constructed using Nextera XT DNA Library Preparation Kit (Illumina) according to the manufacturer's instructions. The libraries were sequenced with 150 bp paired-end reads on the Illumina HiSeq X Ten sequencer (Illumina). Trimmomatic (version 0.33) filtered raw sequenced single-end reads to exclude low-quality sequences (34). The sequenced reads were aligned to the mouse reference genome (mm10) with Hisat2 (version 2.1.0) (35), and the aligned reads were used for the transcript quantification by using featureCounts (version 1.6.5) (36). DESeq2 was used to normalize and identify differentially expressed genes with adjusted $p < 0.3$ (DEGs) (37). The

normalized data was visualized by MA plots and heatmaps using the R package pheatmap (version 1.0.12).

Previous data (GSE99780) of ILC2 in acute and chronic airway inflammation from the paper by Li et al. (38) were reanalyzed using Trimmomatic (version 0.33), Hisat2 (version 2.1.0), featureCounts (version 1.6.5), and pheatmap (version 1.0.12).

Reanalysis of single-cell RNA-sequencing (scRNA-seq) data

Previous data (GSM3575497) of lung CD45^{-} stromal cells from the paper by Dahlgren et al. (16) were reanalyzed using the R package Seurat (4.0.2) and pheatmap (1.0.12) for single-cell RNA-seq analysis (39). Log-normalized gene expression data were used for visualization with UMAP plots and heatmaps for each cluster.

Statistical analysis

All data are presented as mean ± SEM. Comparisons between two samples were performed using an unpaired two-tailed Student's *t*-test. For multiple group comparisons, one-way ANOVA analyses with multiple comparisons were performed using Prism software (8.4.3) (GraphPad). All reported P values were calculated using two-tailed parametric tests, unless otherwise noted. * $p < 0.05$, ** $p < 0.01$, *** $p < 0.001$ and **** $p < 0.0001$.

Data Availability

The accession number for the RNA-seq data of ILC2s in SPC-Cre IL-7cKO mice reported in this paper is GEO: GSE200372.

Results

IL-7 is mainly produced by bronchial epithelial cells, type 2 alveolar epithelial cells, and LECs in the lung

To identify IL-7-producing cells in the lung in steady state, we isolated lung stromal cells from WT mice by cell sorter (Supplementary Figure S1) and analyzed *Il7* transcripts by qRT-PCR. *Il7* transcripts were detected at high levels in LECs, whereas low levels of *Il7* transcripts were also observed in bronchial epithelial cells (bEpi), type 1 alveolar epithelial cells (AEC1s), and type 2 alveolar epithelial cells (AEC2s) (Fig. 1A). To confirm the source of IL-7 in the lung, we next analyzed the lungs of IL-7-GFP reporter mice with anti-GFP antibody by flow cytometry. GFP was highly expressed in LECs, whereas bronchial epithelial cells and type 2 alveolar epithelial cells also expressed GFP at low levels (Fig. 1B). In addition, we analyzed lung sections from IL-7-GFP reporter mice with an anti-GFP antibody by immunohistochemistry. GFP expression was detected in $EpCAM^+$ bronchial epithelial cells and $Lyve1^+$ LECs (Fig. 1C). To further investigate *Il7* gene expression in lung stromal cells in detail, we reanalyzed previously reported single-cell RNA-sequencing (scRNA-seq) data of lung $CD45^-$ cells (16, 40). The lung $CD45^-$ cells were classified into 19 clusters (Fig. 1D). Cluster 16 that expressed the genes *Lyve1*, *Pdpn* (podoplanin), *Prox1,* and *Ccl21a*, in accordance with the characteristics of LECs, highly expressed *Il7* (Fig. 1E, 1F). Cluster 4 that expressed the genes *Epcam*, *Sftpc*, *Nkx2.1*, and *Il33*, consistent with the identity of type 2 alveolar epithelial cells and bronchial epithelial cells, expressed *Il7* at lower levels than cluster 16. These results suggest that IL-7 is expressed at higher levels in LECs and at lower levels in bronchial epithelial cells and type 2 alveolar epithelial cells in the lung.

Localization of lung ILC2s changes during inflammation

ILC2s have been reported to localize in the perivascular space of the lung in steady state and airway inflammation in the vicinity of bronchia, bronchioles, arteries, and lymphatic vessels (16, 17, 19, 31). However, the localization of ILC2s in the lung has not been compared in detail between steady state and airway inflammation. Two types of inflammation were applied to IL-$5^{Venus/+}$ reporter mice to elucidate the difference in the localization of ILC2s in the lung during airway inflammation. First, we administered papain i.n. to the mice to induce airway inflammation and activate ILC2s (Fig. 2A). Second, we sensitized and challenged the mice with HDM to induce allergic airway inflammation by Th2 cells (Fig. 2B). The frequency of IL-5^+ cells in lung ILC2s (lineage$^-$IL-$7R^+CD25^+Sca\text{-}1^+$) was determined by flow cytometry. IL-5-Venus expression was detected in 12~30% of lung ILC2s, and the IL-33 expression level of the whole lung in papain-induced airway inflammation was higher than that in HDM-induced airway inflammation (Supplementary Figure S2A and B). As previously reported (18, 31), $CD3^-$IL-5-$Venus^+$ ILC2s were detected by immunohistochemistry (Fig. 2C). In steady state and papain-induced inflammation, IL-5-$Venus^+$ ILC2s were located closer to airway epithelia than to lymphatic vessels. In contrast, in HDM-induced inflammation, IL-5-$Venus^+$ ILC2s were closer to lymphatic vessels than to airway epithelia. Next, we compared the distance between IL-5-$Venus^+$ ILC2s and bronchia or LECs. IL-5-$Venus^+$ ILC2s localized closer to airway epithelia in steady state and papain-induced inflammation than IL-5-$Venus^+$ ILC2s in HDM-induced inflammation (Fig. 2D and Supplementary Figure S2C and D). Similarly, IL-5-$Venus^+$ ILC2s localized closer to lymphatic vessels in HDM-induced inflammation than IL-5-$Venus^+$ ILC2s in papain-induced inflammation. Therefore, these results suggest that ILC2s localize close to bronchial epithelial layers in steady state and papain-induced airway inflammation but that ILC2s localize close to lymphatic vessels in HDM-induced airway inflammation.

ILC2s differentially express chemokines and chemokine receptors in papain- and HDM-

induced airway inflammation

To investigate the mechanism of differential localization of ILC2s between papain- and HDM-induced inflammation, we reanalyzed previously reported RNA-seq data of lung ILC2s in IL-33-induced and HDM-induced airway inflammation (38). *Ccr4* expression in ILC2s was higher in IL-33-induced acute inflammation than in HDM-induced chronic inflammation, whereas *Ccr2* expression was higher in HDM-induced chronic inflammation than in IL-33-induced acute inflammation (Supplementary Figure S2E). To confirm the chemokine receptor expression, we analyzed *Ccr2* and *Ccr4* mRNA in ILC2s in steady state, papain-induced inflammation, and HDM-induced inflammation. *Ccr4* expression in ILC2s was higher in papain-induced inflammation than in HDM-induced inflammation, whereas *Ccr2* expression in ILC2s was reduced in papain-induced inflammation compared to HDM-induced inflammation (Supplementary Figure S2F). Consistently, CCR4 expression on ILC2s was elevated in papain-induced inflammation (Supplementary Figure S2G).

To investigate whether the chemokine receptor expression affects the localization of ILC2s during inflammation, we administered anti-CCL17 and anti-CCL2 antibodies, which target the ligands of CCR4 and CCR2, respectively, to IL-5-Venus reporter mice and induced papain- and HDM-induced airway inflammation. In the anti-CCL17 antibody-treated mice, the tendency of ILC2 distribution near bronchia was lost, and eosinophil infiltration in the BALF was diminished in papain-induced inflammation (Supplementary Figure S3A-F). On the other hand, in the anti-CCL2 antibody-treated mice, the tendency of ILC2 distribution near lymphatic vessels disappeared, and the frequency of IL-5$^+$ T cells was reduced in HDM-induced inflammation (Supplementary Figure S4A-F). Thus, these results suggest that ILC2s differentially express CCR4 and CCR2 in papain- and HDM-induced airway inflammation. As previously reported (38), ILC2s also expressed *Ccl6* and *Cxcl10* at higher levels in HDM-induced chronic inflammation than in IL-33-induced acute inflammation (Supplementary Figure S2E). Since T cells are one of the target cells for CCL6 and CXCL10, we next examined the distance between ILC2s and T cells. ILC2s localized closer to T cells in HDM-induced inflammation than in steady state (Fig. 2E). These results suggest that ILC2s differentially express chemokines and chemokine receptors in papain- and HDM-induced airway inflammation, which may control the distribution of ILC2s and the interaction between ILC2s and T cells.

In addition to chemokines and chemokine receptors, ILC2s in HDM-induced chronic airway inflammation highly expressed the genes related to memory T cells (*Il7r, Itgae, Il1rl1, Il17re*) and regulatory-like phenotype (*Tgfb1, Tgfbr2*) (Supplementary Figure S2E). On the other hand, ILC2s expressed at lower levels the genes related to exhaustion (*Tigit, Ctla4*), or at different levels the genes related to plasticity (*Tbx21, Rorc*) in HDM-induced chronic inflammation. These results suggest that ILC2s change their functions depending on the type of airway inflammation.

Local IL-7 is dispensable for the maintenance of lung ILC2s in steady state

IL-7 has been reported to be critical for the development and maintenance of ILC2s (24, 41). Although ILC2s are tissue-resident (42), whether local IL-7 affects tissue-resident ILC2s in vivo remains unknown. To investigate the role of lung IL-7 in ILC2s in steady state, we first analyzed SPC-Cre IL-7cKO mice with IL-7 deletion in bronchoalveolar epithelial cells. Lung ILC2s were detected as Lineage$^-$Sca-1$^+$IL-7R$^+$CD25$^+$ cells (Fig. 3A). The number of lung ILC2s was unchanged in SPC-Cre IL-7cKO mice compared to control mice (Fig. 3B, 3C). Next, we analyzed Lyve1-Cre IL-7cKO mice with IL-7 deletion in LECs. The number of ILC2s was also unchanged in Lyve1-Cre IL-7cKO mice compared with control mice (Fig. 3D, 3E). The numbers of other immune cells, such as T cells, B cells, NK cells, and myeloid cells, and the localization of ILC2s were also unchanged in the lung of SPC-Cre and Lyve1-Cre IL-7cKO

mice in steady state (Supplementary Figure S5). These results suggest that local IL-7 produced by bronchoalveolar epithelial cells and LECs is dispensable for maintaining lung ILC2s in steady state.

IL-7 produced by bronchoalveolar epithelial cells promotes ILC2 activation in papain-induced airway inflammation

IL-7 signaling enables the activation of ILC2s in vitro (27). To elucidate the function of IL-7 in airway inflammation, we analyzed SPC-Cre IL-7cKO mice and Lyve1-Cre IL-7cKO mice in papain-induced airway inflammation. Because most IL-5-Venus-expressing cells were $Lin^{-}IL\text{-}7R^{+}Sca\text{-}1^{+}CD25^{+}KLRG1^{+}$ ILC2s, ILC2s were the cells mainly activated to produce IL-5, inducing eosinophilic infiltration in papain-induced inflammation (Supplementary Figure S6A). Because eosinophil infiltration is a sensitive indicator of airway inflammation, we first examined eosinophils in the BALF. The frequency and number of eosinophils were reduced in the BALF of SPC-Cre IL-7cKO mice compared to control mice, whereas alveolar macrophages were unchanged (Fig. 4A). The levels of IL-5 and IL-13 in the BALF were also reduced in SPC-Cre IL-7cKO mice (Fig. 4B). In contrast, the frequency and number of eosinophils and alveolar macrophages in the BALF of Lyve1-Cre IL-7cKO mice were unchanged (Fig. 4C), and the levels of IL-5 and IL-13 in the BALF were also unchanged (Fig. 4D). The numbers of other immune cells including ILC2s were unchanged in SPC-Cre IL-7cKO mice and Lyve1-Cre IL-7cKO mice compared to control mice (Fig. 4E-H and Supplementary Figure S6B and C). IL-5 and IL-13 expression in ILC2s was also unaffected in IL-7cKO mice (Supplementary Figure S6D and E). Lung inflammation was attenuated in SPC-Cre IL7cKO mice, as evidenced by infiltration of leukocytes into the perivascular space and thickened airway epithelia as shown by H&E staining of lung sections (Fig. 5A and Supplementary Figure S7A). In contrast, airway inflammation was unchanged in Lyve1-Cre IL-7cKO mice compared to control mice (Fig. 5B and Supplementary Figure S7B). These results suggest that IL-7 produced by bronchoalveolar epithelial cells exacerbates papain-induced airway inflammation via activation of ILC2s.

To assess the effects of epithelial cell IL-7 on ILC2s in detail, we performed gene expression profiling of ILC2s from SPC-Cre IL-7cKO mice in papain-induced airway inflammation by RNA-seq analysis. We found that several differentially expressed genes related to the activation of ILC2s (*Il5, Il13, Cxcl2, Cxcl3, Hif1a, Cysltr2*) were reduced in ILC2s from SPC-Cre IL-7cKO mice (Fig. 5C and D). As previously reported (27), the addition of IL-7 slightly enhanced the production of IL-5 and IL-13 by ILC2s in response to IL-33 (Supplementary Figure S7C). The expressions of *Il1rl1* (ST2, IL-33R) and *Crlf2* (TSLPR) were reduced in ILC2s of SPC-Cre IL-7cKO mice (Fig. 5D). We also confirmed ST2 protein expression by flow cytometry. ST2 expression on ILC2s was also increased by stimulation with IL-7 and IL-33, but not by IL-33 or IL-7 alone (Fig 5E). These results suggest that the IL-7 signaling upregulates ST2 on ILC2s and enhances IL-5 production and subsequent eosinophil infiltration. ILC2s of SPC-Cre IL-7cKO mice also expressed at lower levels the genes associated with lymphocyte maintenance and differentiation (*Mtor, Hif1a, Il2rb, Runx1, Notch1*) and regulation of T cell functions (*Ctla4, Cd274*) (Fig. 5D). In contrast, ILC2s from SPC-Cre IL-7cKO mice expressed comparable levels of the genes related with chemoattraction of ILC2s (*Ccr2, Ccr4, Ccr7*). The localization of ILC2s in SPC-Cre IL-7cKO and Lyve1-Cre IL-7cKO mice was unchanged in papain-induced airway inflammation (Supplementary Figure. S7D). These results suggest that IL-7 produced by bronchoalveolar epithelial cells supports ILC2 activation by upregulating the genes related to IL-33R in innate immunity-mediated airway inflammation.

IL-7 produced by LECs maintains lung ILC2s in HDM-induced airway inflammation

To investigate the function of local IL-7 in lung ILC2s in HDM-induced airway inflammation,

we analyzed SPC-Cre IL-7cKO mice and Lyve1-Cre IL-7cKO mice. The frequency and number of ILC2s and other immune cells were unchanged in the lung of SPC-Cre IL-7cKO mice compared to control mice (Fig. 6A, 6B and Supplementary Figure S8A). Notably, ILC2s were significantly reduced in Lyve1-Cre IL-7cKO mice (Fig. 6C and 6D). Because resident memory CD4 T cells depend on LEC IL-7 for maintenance (10), we also analyzed CD4 T cells and other immune cells. The numbers of CD4 T cells and other immune cells were unchanged in the lung of Lyve1-Cre IL-7cKO mice (Fig. 6D and Supplementary Figure S8B). To analyze the mechanism of the reduction of ILC2s in Lyve1-Cre IL-7cKO mice, we stained ILC2s for an anti-apoptotic protein, Bcl-2, and a proliferation-related protein, Ki-67. The expressions of Bcl-2 and Ki-67 were reduced in ILC2s of Lyve1-Cre IL-7cKO mice compared to control mice (Fig. 6E and 6F). Bcl-2 and Ki-67 were unchanged in SPC-Cre IL-7cKO mice (Supplementary Figure S8C).

Next, we confirmed whether IL-7 activates type 2 inflammation in HDM-induced inflammation. Eosinophils, alveolar macrophages, and type 2 cytokines in the BALF were unchanged in SPC-Cre and Lyve1-Cre IL-7cKO mice (Fig. 6G-J). IL-5 and IL-13 expression in ILC2s was also unaffected in IL-7cKO mice (Supplementary Figure S8D and E). The localization of ILC2s appeared unchanged in SPC-Cre IL-7cKO mice and Lyve1-Cre IL-7cKO mice (Supplementary Figure. 8F). Inflammatory signatures analyzed by H&E staining of lung sections were also unaffected (Supplementary Figure 9A-D). These results suggest that local IL-7 does not affect the activation of ILC2s in HDM-induced airway inflammation. Moreover, to confirm differences in the expression of IL-7 on stromal cells between steady state, papain-induced, and HDM-induced inflammation, we analyzed IL-7-GFP reporter mice. However, GFP expressions were unchanged between conditions (Supplementary Figure S10). These results suggest that IL-7 produced by LECs supports the survival and proliferation of ILC2s in HDM-induced airway inflammation due to their localization close to lymphatic vessels.

Anti-IL-7 antibody treatment attenuates papain-induced airway inflammation by inhibiting ILC2 activation

Anti-IL-7 or anti-IL-7Rα antibodies reportedly block IL-7 signaling and ameliorate airway inflammation (43, 44). To test whether anti-IL-7 antibody alleviates airway inflammation via ILC2s, we treated WT mice with anti-IL-7 antibody in papain-induced inflammation (Fig. 7A). The frequency and number of eosinophils were significantly reduced in the BALF of anti-IL-7 antibody-treated mice compared to the isotype control, whereas the frequency of alveolar macrophages was increased (Fig. 7B). The concentration of IL-5 was also reduced in the BALF of anti-IL-7 antibody-treated mice (Fig. 7C). Furthermore, the expressions of IL-5 and IL-13 in lung ILC2s were slightly decreased in anti-IL-7 antibody-treated mice, although the number of ILC2s and other immune cells in the lung was unchanged (Fig. 7D, 7E, and Supplementary Figure S11). Histological analysis with H&E staining revealed that anti-IL-7 antibody treatment dramatically attenuated papain-induced inflammation, with reduced immune cell infiltration into the perivascular and peribronchial spaces and thinner airway walls (Fig. 7F). Moreover, ST2 expression was decreased in lung ILC2s of anti-IL-7 antibody-treated mice (Fig. 7G). These results suggest that anti-IL-7 antibody treatment alleviates innate immunity-mediated airway inflammation by inhibiting ILC2 activation.

Discussion

In this study, we determined the role of lung IL-7 in the distribution, activation, and maintenance of ILC2s in steady state and airway inflammation using cell type-specific IL-7 cKO mice. IL-7 is required for the development, maintenance, and activation of ILCs. However, whether local IL-7 affects the functions of ILC2s in peripheral tissues remains unknown. This study found that lung LECs and bronchoalveolar epithelial cells are major producers of IL-7. In steady state and papain-induced airway inflammation, ILC2s are located near bronchia and bronchioles. In contrast, in HDM-induced airway inflammation, ILC2s reside close to lymphatic vessels. Consistently, IL-5 production and inflammation are attenuated in papain-induced airway inflammation in bronchoalveolar epithelial cell-specific SPC-Cre IL-7cKO mice. In contrast, in HDM-induced airway inflammation, the number of ILC2s and the expression of Bcl-2 and Ki-67 in ILC2s are reduced in LEC-specific Lyve1-Cre IL-7cKO mice. Since papain-induced inflammation depends on IL-33 from epithelial cells, the localization of ILC2s near epithelial cells makes sense. On the other hand, since HDM-induced inflammation depends on antigen-specific T cells, the localization of ILC2s near T cells and LECs is understandable. These results suggest that IL-7 produced by different stromal cells controls ILC2s depending on the type of airway inflammation.

In steady state, lung ILC2s do not appear to require local IL-7 for their maintenance (Fig. 3C and 3E). Cytokines other than IL-7 may support the maintenance of ILC2s in the lung parenchyma. Since ILC2s are located near airway epithelia in steady state (Fig. 2C, 2D, and Supplementary Figure S2C and D), it is conceivable that ILC2s receive cytokines from the adjacent airway epithelial cells. Lung bronchoalveolar epithelial cells produce IL-33, TSLP, and IL-25 during airway inflammation, which may play a role in the maintenance and cytokine production of ILC2s (17, 24, 27). Although these cytokines are mainly secreted during inflammation, they are likely to be produced at low levels, even in steady state, which may contribute to the maintenance of lung ILC2s without IL-7.

In papain-induced airway inflammation, ILC2s appear to be potentiated by IL-7 produced by bronchoalveolar epithelial cells. ILC2s are reported to be stimulated by IL-2, IL-7, and TSLP in vitro (27, 28). These cytokines activate STAT5, which induces GATA3 expression and thus IL-5 and IL-13 production in ILC2s (26, 45, 46). However, whether these cytokines, especially IL-7, can activate ILC2s in vivo is unknown. In this study, the expression of type 2 cytokines and the genes related to lymphocyte activation was reduced in ILC2s of SPC-Cre IL-7cKO mice (Fig. 4B, 5C, and 5D). In addition, IL-2 and TSLP have been reported to induce ST2 expression on Th2 cells (47). The expression of IL-33R (ST2, *Il1rl1*) and TSLPR (*Crlf2*) was reduced in ILC2s of SPC-Cre IL-7cKO mice (Fig. 5C and D), suggesting that IL-7 signaling in ILC2s induces the expression of IL-33R and TSLPR. Therefore, IL-7 may enhance the type 2 cytokine production of ILC2s by upregulating the expression of ST2 and TSLPR. As for the signaling pathway by which IL-7 upregulates ST2 expression, since IL-2 or TSLP stimulation activates STAT5, which upregulates GATA3 expression and thereby ST2 expression (47), IL-7, which also activates STAT5, may induce ST2 expression in a similar pathway.

In HDM-induced airway inflammation, ILC2s appear to be maintained, at least in part, by IL-7 produced by LECs (Fig. 6D), based on their localization close to LECs (Fig. 2D). In the HDM-induced airway inflammation model, it is conceivable that Th2 cells, as well as ILC2s, produce IL-5 and IL-13. Memory Th2 cells are reduced in the lung of Tie2-Cre IL-7cKO mice, in which IL-7 is deleted from endothelial cells one month after the adoptive transfer of effector Th2 cells, suggesting that LEC IL-7 is required for maintenance of memory Th2 cells (10). However, in our HDM-induced model, tissue-resident memory T cells may not be induced in the airway by intraperitoneal injection for sensitization, which may explain the reason why tissue-resident memory T cells were unchanged in Lyve1-Cre IL-7cKO mice.

From a previous report and our reanalysis of RNA-seq data, ILC2s in HDM-induced chronic airway inflammation exhibit a unique phenotype (Supplementary Figure S2E) (38). Compared to those in IL-33-induced acute airway inflammation, ILC2s in HDM-induced airway inflammation highly expressed the genes related to memory T cells (*Il7r, Itgae, Il1rl1, Il17re*) and regulatory-like phenotype (*Tgfb1, Tgfbr2*). In contrast, they expressed at lower levels the genes related to exhaustion (*Tigit, Ctla4*). Thus, ILC2s in HDM-induced airway inflammation have different phenotypes and functions than 'naive' ILC2s, with a memory- or regulatory-like phenotype but less exhaustion. Interestingly, NK cells can have memory-like functions during viral infection (48, 49). Thus, the memory-like features of NK cells and ILC2 in chronic infection and inflammation may share a mechanism with memory T cells. This will be an intriguing question in the future.

We found that ILC2s tend to localize near bronchia or bronchioles in steady state and papain-induced airway inflammation (Fig. 2C, 2D). ILC2s are located in peribronchial and perivascular spaces close to airway epithelia, lymphatic vessels, and arteries in steady state (16-18, 38). In addition, ILC2s increase in perivascular and peribronchial regions during airway inflammation (19, 20). The major difference between the previous reports and this study is that in this study, the ILC2 localization was quantitatively analyzed and compared between different conditions and different IL-7 cKO mice. The bronchoalveolar epithelial cells can produce IL-33, IL-25, and TSLP, which support the survival, proliferation, and cytokine production of ILC2s (12-14). Therefore, it is reasonable that lung ILC2s localize close to airway epithelia in steady state. Moreover, because ILC2s highly express CCR4 in papain-induced airway inflammation (Supplementary Figure S2E, S2F), they could be attracted to the bronchoalveolar epithelial cells that produce its ligand CCL17. Thus, it is possible that ILC2s located near airway epithelia rapidly induce IL-5 and eosinophil infiltration upon epithelial cell damage.

On the other hand, few studies have reported the localization of ILC2s in HDM-induced airway inflammation. ILC2s are close to T cell clusters and may regulate T cell function in HDM-induced airway inflammation (38). We showed that ILC2s tend to be located near lymphatic vessels and T cells in HDM-induced airway inflammation (Fig. 2C, 2D, 2E). Since ILC2s highly express CCR2 in HDM-induced airway inflammation (Supplementary Figure S2F), they may be attracted to the LECs that produce its ligand CCL2. Thus, ILC2s near lymphatic vessels may receive survival signals of IL-7 from the LECs. In addition, ILC2s reside closer to T cells than LECs in HDM-induced airway inflammation (Fig. 2D, 2E), suggesting that ILC2s may interact with T cells with specific functions. Several groups have reported that T cells and ILC2s contact each other (50, 51). However, the subset of T cells that interact with ILC2s in HDM-induced airway inflammation remains unknown. Inducible bronchial-associated lymphoid tissue, iBALT, characterized by $Thy1^+$ IL-7-producing LECs, has been reported to support the maintenance of memory Th2 cells (51). Thus, ILC2s appear to contact T cells entered from lymph and resident memory Th2 cells near lymphatic vessels in HDM-induced airway inflammation. After repeated antigen challenges, rapidly activated ILC2s may help activate Th2 cells via cytokines, thereby amplifying the type 2 response. Another possibility is that Treg cells contact ILC2s in HDM-induced airway inflammation. Treg cells are reported to suppress ILC2s through ICOS-ICOSL interaction (52). *Icosl*, *Cd86*, *and Cd274* (PDL-1) were highly expressed on ILC2s in HDM-induced airway inflammation (Supplementary Figure S2E), suggesting that Treg cells expressing ICOS, CTLA4, and PD-1 interact with ILC2s to suppress their functions. Further studies are needed to identify the T cell subset that interacts with ILC2s in adaptive immunity-mediated airway inflammation.

We have shown that the CCR4-CCL17 and CCR2-CCL2 axes regulate the localization of ILC2s in papain- and HDM-induced inflammation, respectively. However, the mechanism of how these chemokines are specifically produced by bronchial epithelial cells or LECs during inflammation is still unclear. In future studies, it would be helpful to confirm whether CCL17

expressed by bronchial epithelial cells in papain-induced inflammation and CCL2 expressed by LECs in HDM-induced inflammation are higher than the steady state. It is also unclear how papain- and HDM-induced inflammation specifically induces changes in CCR4 and CCR2 expression on ILC2s, respectively.

Moreover, some ILC2s are not tissue resident but migratory. Intestinal ILC2s migrate from the gut to the lung or mesenteric lymph nodes upon IL-25 stimulation or helminth infection (53). Bone marrow ILC2 progenitors migrate to the lungs in fungal allergic airway inflammation (54). Therefore, ILC2s in local tissues may have different and unique phenotypes and sometimes help other tissues. We showed that lung ILC2s localize close to lymphatic vessels in HDM-induced airway inflammation, and ILC2s in HDM-induced airway inflammation have a different phenotype from ILC2s in IL-33-induced acute airway inflammation. One hypothesis is that ILC2s may not change their phenotype in the local lung parenchyma, but ILC2s from other tissues may migrate to the lung in HDM-induced inflammation. However, the source of ILC2s in HDM-induced inflammation remains unknown. Thus, it will be necessary to clarify where ILC2s come from and how they acquire the distinct phenotype in adaptive immunity-mediated airway inflammation.

Administration of anti-IL-7 antibody remarkably suppressed eosinophil infiltration in papain-induced airway inflammation (Fig. 7). It is conceivable that ILC2s are mainly activated in papain-induced inflammation. We injected the anti-IL-7 antibody once, resulting in specific suppression of ILC2 activation in the short term. Therefore, these results suggest that anti-IL-7 antibody treatment alleviates papain-induced airway inflammation by suppressing ILC2 activation. However, anti-IL-7 antibody administration adversely affects lymphocyte development and function in the long term. Anti-IL-7 antibody administration reduces T and B cells in chronic airway inflammation (44). Thus, further studies are needed to confirm the systemic effects of anti-IL-7 antibodies in the long term.

In conclusion, our study demonstrates that lung IL-7 plays an essential role in the distribution, activation, and maintenance of lung ILC2s. In papain-induced airway inflammation, ILC2s tend to localize close to bronchoalveolar epithelial cells and receive IL-7 for activation. In contrast, in HDM-induced airway inflammation, ILC2s localize close to LECs and receive IL-7 for proliferation and survival. Furthermore, anti-IL-7 antibody treatment alleviates papain-induced airway inflammation by suppressing ILC2s. Thus, this study provides new insights into the local functions of lung IL-7 in ILC2s in innate and adaptive immunity-mediated airway inflammation and proposes a novel therapeutic target for airway inflammation.

Funding
This work was supported by the Japan Society for the Promotion of Science (JSPS) KAKENHI grant numbers 20H03501 and 20K21525 (K.I.); by a grant from Takeda Science Foundation to A.S.; by grants from the Shimizu Foundation for Immunology and Neuroscience to A.S. and S.T.; and by the Joint Usage/Research Center program of Institute for Frontier Life and Medical Sciences Kyoto University. D.T. was supported by Fujita Jinsei Scholarship from the Faculty of Pharmaceutical Sciences, Kyoto University, and by the Research Assistant (RA) Program of the Kyoto University Graduate Program for Medical Innovation from the Ministry of Education, Culture, Sports, Science and Technology, and the Japan Society for the Promotion of Science.

Acknowledgements
We thank Dr. J. Cyster for Lyve1-Cre mice, Mr. H. Miyachi and Ms. S. Kitano for manipulation of mouse embryos, and members of the K. Ikuta laboratory for discussion. We thank the Medical Research Support Center and the Innovative Support Alliance for Life Science for the Imaris image analysis software.

References

1 Patton, D. T., Plumb, A. W., Redpath, S. A. *et al.* 2014. The development and survival but not function of follicular B cells is dependent on IL-7Rα Tyr449 signaling. *PLoS One* 9:e88771.

2 Park, J. H., Adoro, S., Guinter, T. *et al.* 2010. Signaling by intrathymic cytokines, not T cell antigen receptors, specifies CD8 lineage choice and promotes the differentiation of cytotoxic-lineage T cells. *Nat. Immunol.* 11:257.

3 Tan, J. T., Dudl, E., LeRoy, E. *et al.* 2001. IL-7 is critical for homeostatic proliferation and survival of naive T cells. *Proc. Natl. Acad. Sci. USA* 98:8732.

4 Surh, C. D. and Sprent, J. 2008. Homeostasis of naive and memory T cells. *Immunity* 29:848.

5 von Freeden-Jeffry, U., Vieira, P., Lucian, L. A. *et al.* 1995. Lymphopenia in interleukin (IL)-7 gene-deleted mice identifies IL-7 as a nonredundant cytokine. *J. Exp. Med.* 181:1519.

6 Peschon, J. J., Morrissey, P. J., Grabstein, K. H. *et al.* 1994. Early lymphocyte expansion is severely impaired in interleukin 7 receptor-deficient mice. *J. Exp. Med.* 180:1955.

7 Jiang, Q., Li, W. Q., Aiello, F. B. *et al.* 2005. Cell biology of IL-7, a key lymphotrophin. *Cytokine Growth Factor Rev.* 16:513.

8 Tani-ichi, S., Shimba, A., Wagatsuma, K. *et al.* 2013. Interleukin-7 receptor controls development and maturation of late stages of thymocyte subpopulations. *Proc. Natl. Acad. Sci. USA* 110:612.

9 Hara, T., Shitara, S., Imai, K. *et al.* 2012. Identification of IL-7-producing cells in primary and secondary lymphoid organs using IL-7-GFP knock-in mice. *J. Immunol.* 189:1577.

10 Shinoda, K., Hirahara, K., Iinuma, T. *et al.* 2016. Thy1^{+}IL-7^{+} lymphatic endothelial cells in iBALT provide a survival niche for memory T-helper cells in allergic airway inflammation. *Proc. Natl. Acad. Sci. USA* 113:E2842.

11 Klose, C. S. and Artis, D. 2016. Innate lymphoid cells as regulators of immunity, inflammation and tissue homeostasis. *Nat. Immunol.* 17:765.

12 Barlow, J. L., Peel, S., Fox, J. *et al.* 2013. IL-33 is more potent than IL-25 in provoking IL-13-producing nuocytes (type 2 innate lymphoid cells) and airway contraction. *J. Allergy Clin. Immunol.* 132:933.

13 Kabata, H., Moro, K., Koyasu, S., and Asano, K. 2015. Group 2 innate lymphoid cells and asthma. *Allergol. Int.* 64:227.

14 Kabata, H., Moro, K., and Koyasu, S. 2018. The group 2 innate lymphoid cell (ILC2) regulatory network and its underlying mechanisms. *Immunol. Rev.* 286:37.

15 Vivier, E., Artis, D., Colonna, M. *et al.* 2018. Innate lymphoid cells: 10 years on. *Cell* 174:1054.

16 Dahlgren, M. W., Jones, S. W., Cautivo, K. M. *et al.* 2019. Adventitial stromal cells define group 2 innate lymphoid cell tissue niches. *Immunity* 50:707.

17 Nussbaum, J. C., Van Dyken, S. J., von Moltke, J. *et al.* 2013. Type 2 innate lymphoid cells control eosinophil homeostasis. *Nature* 502:245.

18 Ikutani, M., Tsuneyama, K., Kawaguchi, M. *et al.* 2017. Prolonged activation of IL-5-producing ILC2 causes pulmonary arterial hypertrophy. *JCI Insight* 2:e90721.

19 Sui, P., Wiesner, D. L., Xu, J. *et al.* 2018. Pulmonary neuroendocrine cells amplify allergic asthma responses. *Science* 360.

20 Puttur, F., Denney, L., Gregory, L. G. *et al.* 2019. Pulmonary environmental cues drive group 2 innate lymphoid cell dynamics in mice and humans. *Sci. Immunol.* 4:eaav7638.

21 Robinette, M. L., Fuchs, A., Cortez, V. S. *et al.* 2015. Transcriptional programs define molecular characteristics of innate lymphoid cell classes and subsets. *Nat. Immunol.* 16:306.

22 Panina-Bordignon, P., Papi, A., Mariani, M. *et al.* 2001. The C-C chemokine receptors

CCR4 and CCR8 identify airway T cells of allergen-challenged atopic asthmatics. *J. Clin. Invest.* 107:1357.
23 Knipfer, L., Schulz-Kuhnt, A., Kindermann, M. *et al.* 2019. A CCL1/CCR8-dependent feed-forward mechanism drives ILC2 functions in type 2-mediated inflammation. *J. Exp. Med.* 216:2763.
24 Moro, K., Yamada, T., Tanabe, M. *et al.* 2010. Innate production of T_H2 cytokines by adipose tissue-associated c-Kit$^+$Sca-1$^+$ lymphoid cells. *Nature* 463:540.
25 Robinette, M. L., Bando, J. K., Song, W. *et al.* 2017. IL-15 sustains IL-7R-independent ILC2 and ILC3 development. *Nat. Commun.* 8:14601.
26 Sheikh, A. and Abraham, N. 2019. Interleukin-7 receptor alpha in innate lymphoid cells: more than a marker. *Front. Immunol.* 10:2897.
27 Halim, T. Y., Krauss, R. H., Sun, A. C., and Takei, F. 2012. Lung natural helper cells are a critical source of Th2 cell-type cytokines in protease allergen-induced airway inflammation. *Immunity* 36:451.
28 Mohapatra, A., Van Dyken, S. J., Schneider, C. *et al.* 2016. Group 2 innate lymphoid cells utilize the IRF4-IL-9 module to coordinate epithelial cell maintenance of lung homeostasis. *Mucosal Immunol.* 9:275.
29 Xu, W., Domingues, R. G., Fonseca-Pereira, D. *et al.* 2015. NFIL3 orchestrates the emergence of common helper innate lymphoid cell precursors. *Cell Rep.* 10:2043.
30 Liang, B., Hara, T., Wagatsuma, K. *et al.* 2012. Role of hepatocyte-derived IL-7 in maintenance of intrahepatic NKT cells and T cells and development of B cells in fetal liver. *J. Immunol.* 189:4444.
31 Ikutani, M., Yanagibashi, T., Ogasawara, M. *et al.* 2012. Identification of innate IL-5-producing cells and their role in lung eosinophil regulation and antitumor immunity. *J. Immunol.* 188:703.
32 Hato, T., Kimura, Y., Morisada, T. *et al.* 2009. Angiopoietins contribute to lung development by regulating pulmonary vascular network formation. *Biochem. Biophys. Res. Commun.* 381:218.
33 Pham, T. H., Baluk, P., Xu, Y. *et al.* 2010. Lymphatic endothelial cell sphingosine kinase activity is required for lymphocyte egress and lymphatic patterning. *J. Exp. Med.* 207:17.
34 Bolger, A. M., Lohse, M., and Usadel, B. 2014. Trimmomatic: a flexible trimmer for Illumina sequence data. *Bioinformatics* 30:2114.
35 Kim, D., Langmead, B., and Salzberg, S. L. 2015. HISAT: a fast spliced aligner with low memory requirements. *Nat. Methods* 12:357.
36 Liao, Y., Smyth, G. K., and Shi, W. 2014. featureCounts: an efficient general purpose program for assigning sequence reads to genomic features. *Bioinformatics* 30:923.
37 Anders, S. and Huber, W. 2010. Differential expression analysis for sequence count data. *Genome Biol.* 11:R106.
38 Li, B. W. S., Stadhouders, R., de Bruijn, M. J. W. *et al.* 2017. Group 2 innate lymphoid cells exhibit a dynamic phenotype in allergic airway inflammation. *Front. Immunol.* 8:1684.
39 Satija, R., Farrell, J. A., Gennert, D. *et al.* 2015. Spatial reconstruction of single-cell gene expression data. *Nat. Biotechnol.* 33:495.
40 Niethamer, T. K., Stabler, C. T., Leach, J. P. *et al.* 2020. Defining the role of pulmonary endothelial cell heterogeneity in the response to acute lung injury. *Elife* 9:e53072.
41 Koga, S., Hozumi, K., Hirano, K. I. *et al.* 2018. Peripheral PDGFRα^+gp38$^+$ mesenchymal cells support the differentiation of fetal liver-derived ILC2. *J. Exp. Med.* 215:1609.
42 Moro, K., Kabata, H., Tanabe, M. *et al.* 2016. Interferon and IL-27 antagonize the function of group 2 innate lymphoid cells and type 2 innate immune responses. *Nat. Immunol.* 17:76.
43 Grabstein, K. H., Waldschmidt, T. J., Finkelman, F. D. *et al.* 1993. Inhibition of murine B and T lymphopoiesis in vivo by an anti-interleukin 7 monoclonal antibody. *J. Exp. Med.*

178:257.
44 Mai, H. L., Nguyen, T. V. H., Bouchaud, G. *et al.* 2020. Targeting the interleukin-7 receptor alpha by an anti-CD127 monoclonal antibody improves allergic airway inflammation in mice. *Clin. Exp. Allergy* 50:824.
45 Zhong, C., Cui, K., Wilhelm, C. *et al.* 2016. Group 3 innate lymphoid cells continuously require the transcription factor GATA-3 after commitment. *Nat. Immunol.* 17:169.
46 Mjosberg, J., Bernink, J., Golebski, K. *et al.* 2012. The transcription factor GATA3 is essential for the function of human type 2 innate lymphoid cells. *Immunity* 37:649.
47 Guo, L., Wei, G., Zhu, J. *et al.* 2009. IL-1 family members and STAT activators induce cytokine production by Th2, Th17, and Th1 cells. *Proc. Natl. Acad. Sci. USA* 106:13463.
48 Cooper, M. A., Elliott, J. M., Keyel, P. A. *et al.* 2009. Cytokine-induced memory-like natural killer cells. *Proc. Natl. Acad. Sci. USA* 106:1915.
49 Lee, J., Zhang, T., Hwang, I. *et al.* 2015. Epigenetic modification and antibody-dependent expansion of memory-like NK cells in human cytomegalovirus-infected individuals. *Immunity* 42:431.
50 Halim, T. Y., Steer, C. A., Matha, L. *et al.* 2014. Group 2 innate lymphoid cells are critical for the initiation of adaptive T helper 2 cell-mediated allergic lung inflammation. *Immunity* 40:425.
51 Mirchandani, A. S., Besnard, A. G., Yip, E. *et al.* 2014. Type 2 innate lymphoid cells drive $CD4^+$ Th2 cell responses. *J. Immunol.* 192:2442.
52 Rigas, D., Lewis, G., Aron, J. L. *et al.* 2017. Type 2 innate lymphoid cell suppression by regulatory T cells attenuates airway hyperreactivity and requires inducible T-cell costimulator-inducible T-cell costimulator ligand interaction. *J. Allergy Clin. Immunol.* 139:1468.
53 Huang, Y., Mao, K., Chen, X. *et al.* 2018. S1P-dependent interorgan trafficking of group 2 innate lymphoid cells supports host defense. *Science* 359:114.
54 Karta, M. R., Rosenthal, P. S., Beppu, A. *et al.* 2018. β2 integrins rather than β1 integrins mediate *Alternaria*-induced group 2 innate lymphoid cell trafficking to the lung. *J. Allergy Clin. Immunol.* 141:329.

Figure legends

Figure 1. Bronchial epithelial cells, type 2 alveolar epithelial cells, and LECs are major producers of IL-7 in the lung.
(**A**) qRT-PCR analysis of *Il7* mRNA expression in bronchial epithelial cells (bEpi), type 1 alveolar epithelial cells (AEC1s), type 2 alveolar epithelial cells (AEC2s), blood vascular endothelial cells (BECs), LECs, and macrophages. Expression levels were normalized to HPRT (n = 3). (**B**) GFP expression in the indicated cells of IL-$7^{GFP/+}$ or IL-$7^{+/+}$ mice was analyzed by flow cytometry. (**C**) Lung tissue samples from IL-$7^{GFP/+}$ or IL-$7^{+/+}$ mice were stained with anti-EpCAM (yellow), anti-Lyve1 (cyan), and anti-GFP (red) antibodies. Data represent two to four independent experiments with similar results (B, C). Scale bar, 100 μm. (**D**) Unsupervised clustering reanalysis of scRNAseq data (GSM3688759) of lung $CD45^-$ cells using UMAP. Each dot represents a single cell. (**E**) Heatmap of mean expression values of selected genes related to lung stromal cells. (**F**) IL-7 mRNA expression in each cluster was identified from the scRNA-seq data. Data are mean ± SEM with one-way ANOVA and pooled from 2 independent experiments (A).

Figure 2. Localization of pulmonary ILC2s changes during inflammation.
(**A**) Experimental protocol of papain-induced airway inflammation. Mice were administered i.n. with papain on days 0, 1, and 2 and analyzed on day 3. (**B**) Experimental protocol of house dust mite (HDM)-induced airway inflammation. Mice were administered i.p. with HDM on days 0 and 14, then challenged i.n. with HDM on days 21, 22, and 23, and analyzed on day 37. (**C**) Lung tissue samples (30 μm thickness) from IL-$5^{Venus/+}$ mice were stained with anti-EpCAM (yellow, bronchial structure), anti-Lyve1 (green, lymphatic vessels), anti-GFP (red, IL-5^+ ILC2s) and anti-CD3 (blue, T cells) antibodies. Images are representative of three or more mice. Scale bar, 100 μm. (**D**) Distance between ILC2s and bronchia or LECs in steady state (Steady), papain-induced airway inflammation (Papain), and HDM-induced airway inflammation (HDM). (**E**) Distance between ILC2s and T cells ($CD3^+$). Data points were taken from mice with more than three animals with more than 20 cells of each type analyzed per mouse (D, E). Data are mean ± SEM with one-way ANOVA (E) or Student's *t*-test (D) and pooled from 2-3 independent experiments (D, E). $*p < 0.05$, $**p < 0.01$, $***p < 0.001$.

Figure 3. IL-7 derived from bronchial epithelial cells and LECs is dispensable for maintaining ILC2s in steady state.
(**A**) Gating strategy of ILC2s ($Lineage^-Sca\text{-}1^+IL\text{-}7R^+CD25^+$). (**B**) Flow cytometric analysis of lung ILC2s in control and SPC-Cre IL-7cKO mice. The data represent two independent experiments with similar results. (**C**) The absolute number of lung ILC2s in control and SPC-Cre IL-7cKO mice (n = 5). (**D**) Flow cytometric analysis of lung ILC2s in control and Lyve1-Cre IL-7cKO mice. The data represent two independent experiments with similar results. (**E**) The absolute number of lung ILC2s in control and Lyve1-Cre IL-7cKO mice (n = 6). Data are mean ± SEM with Student's *t*-test and pooled from 2-3 independent experiments (C, E).

Figure 4. Papain-induced airway inflammation depends on IL-7 produced by lung epithelial cells.
Papain-induced airway inflammation was performed as shown in Fig. 2A. (**A**) Frequency and absolute numbers of eosinophils and alveolar macrophages (AM) in the BALF from control and SPC-Cre IL-7cKO mice in papain-induced airway inflammation (n = 7). (**B**) IL-5 and IL-13 levels in the BALF from control or SPC-Cre IL-7cKO mice by ELISA (n = 4-5). (**C**) Frequency and absolute numbers of eosinophils and alveolar macrophages (AM) in the BALF from control or Lyve1-Cre IL-7cKO mice in papain-induced airway inflammation (n = 7). (**D**)

IL-5 and IL-13 concentrations in the BALF from control or Lyve1-Cre IL-7cKO mice by ELISA (n = 3). (**E**) Flow cytometric analysis of lung ILC2s in control and SPC-Cre IL-7cKO mice in papain-induced inflammation. The data represent two independent experiments with similar results. (**F**) Absolute numbers of lung ILC2s, T cells, and total cells in control and SPC-Cre IL-7cKO mice (n = 3). (**G**) Flow cytometric analysis of lung ILC2s in control and Lyve1-Cre IL-7cKO mice in papain-induced inflammation. The data represent two independent experiments with similar results. (**H**) Absolute numbers of lung ILC2s, T cells, and total cells in control and Lyve1-Cre IL-7cKO mice (n = 4). Data are mean ± SEM with Student's *t*-test and pooled from 2-3 independent experiments (A-D, F, and H). **p* < 0.05, ***p* < 0.01.

Figure 5. ILC2 activation in papain-induced airway inflammation depends on IL-7 produced by lung epithelial cells.
(**A**, **B**) Representative lung sections of 10 μm thickness stained with H&E in control and SPC-Cre IL-7cKO mice (A) and in control and Lyve1-Cre IL-7cKO mice (B) (n = 3). Arrows indicate leukocyte infiltration. (**C, D**) MA plot (C) and heat map (D) of selected genes of lung ILC2s from control and SPC-Cre IL-7cKO mice (n = 3). (**E**) Flow cytometric analysis and mean fluorescence intensity (MFI) of ST2 expression on ILC2s ($Lineage^{-}IL\text{-}7R^{+}CD25^{+}Sca\text{-}1^{+}$, 5×10^{3}/well) cultured with the indicated cytokines for three days (n = 4). Data are mean ± SEM with one-way ANOVA and pooled from 2-3 independent experiments (E). ***p* < 0.01, ****p* < 0.001.

Figure 6. IL-7 produced by LECs maintains ILC2 in HDM-induced airway inflammation.
HDM-induced airway inflammation was performed as shown in Fig. 2B. (**A**) Flow cytometric analysis of ILC2s from lung parenchyma of control and SPC-Cre IL-7cKO mice. The data represent two independent experiments with similar results. (**B**) Absolute numbers of ILC2, T cells, and total cells (n = 4). (**C**) Flow cytometric analysis of ILC2s from lung parenchyma of control and Lyve1-Cre IL-7cKO mice. The data represent two independent experiments with similar results. (**D**) Absolute numbers of ILC2, T cells, and total cells (n = 3-6). (**E**) Flow cytometric analysis (*left*) and mean fluorescence intensity (MFI) (*right*) of intracellular staining of Bcl-2 in ILC2s from control and Lyve1-Cre IL-7cKO mice. (**F**) Flow cytometric analysis (*left*) and MFI (*right*) of intracellular staining of Ki-67 in ILC2s from control and Lyve1-Cre IL-7cKO mice. (**G**) Absolute numbers of eosinophils and alveolar macrophages (AM) in the BALF from control and SPC-Cre IL-7cKO mice (n = 3). (**H**) IL-5 and IL-13 concentrations in the BALF from control or SPC-Cre IL-7cKO mice by ELISA (n = 4). (**I**) Absolute numbers of eosinophils and alveolar macrophages (AM) in the BALF from control or Lyve1-Cre IL-7cKO mice (n = 4). (**J**) IL-5 and IL-13 concentrations in the BALF from control or Lyve1-Cre IL-7cKO mice by ELISA (n = 8). Data are mean ± SEM with Student's *t*-test and pooled from 2-3 independent experiments (B-J). **p* < 0.05.

Figure 7. Anti-IL-7 antibody treatment suppresses papain-induced airway inflammation by inhibiting ILC2 activation.
(**A**) Experimental protocol to attenuate papain-induced airway inflammation by the anti-IL-7 antibody. Mice were i.p. treated with anti-IL-7 monoclonal antibody (IL-7mab) or isotype control on day 0, i.n. treated with papain after 3 hours, i.n. treated with papain on days 1 and 2 and analyzed on day 3. (**B**) Frequency and absolute numbers of eosinophils and alveolar macrophages (AM) in the BALF from control or anti-IL-7 antibody-treated mice (n = 7). (**C**) IL-5 (n = 8) and IL-13 (n = 4) levels in the BALF from control or anti-IL-7 antibody-treated mice were analyzed by ELISA. (**D**) The absolute number of ILC2s in the lung parenchyma (n = 10). (**E**) Mean fluorescence intensity (MFI) of IL-5 and IL-13 expression in ILC2s by intracellular staining (n = 9). (**F**) Representative lung sections 10 μm thick stained with H&E

in control or anti-IL-7 antibody-treated mice (n = 4). (**G**) MFI of ST2 expression on ILC2s in the lung parenchyma (n = 9). Data are mean ± SEM with Student's *t*-test and pooled from 2-3 independent experiments (B-E and G). *$p < 0.05$.

Supplementary Figure Legends

Supplementary Figure 1. Gating strategy for lung stromal cells.
Gating strategy for bronchial epithelial cells (bEpi; CD45$^-$Ter119$^-$EpCAM$^+$MHC2$^+$), type1 alveolar epithelial cells (AEC1s; CD45$^-$Ter119$^-$EpCAM$^-$podoplanin$^+$), type 2 alveolar epithelial cells (AEC2s; CD45$^-$Ter119$^-$CD31$^-$EpCAM$^+$MHC2^{high}), lymphatic endothelial cells (LECs; CD45$^-$Ter119$^-$EpCAM$^-$CD31$^+$podoplanin$^+$) and blood vascular endothelial cells (BECs; CD45$^-$Ter119$^-$EpCAM$^-$CD31$^+$podoplanin$^-$) in the lung parenchymal cells is shown.

Supplementary Figure 2. Localization of IL-5-Venus$^+$ ILC2s in steady state and airway inflammation.
(**A**) Flow cytometric analysis of Venus expression in lung ILC2s (Lineage$^-$Sca-1$^+$IL-7R$^+$CD25$^+$) of IL-5$^{Venus/+}$ mice in steady state (Steady), papain-induced airway inflammation (Papain), and HDM-induced airway inflammation (HDM). Data represent three to five independent experiments with similar results. (**B**) qRT-PCR analysis of *Il33* expression in the whole lung. (**C**) The proportion of ILC2s with indicated distance from the bronchial epithelium (Bronchia) or lymphatic vessels (LEC). Data points were obtained from more than 20 cells per mouse and more than three mice. (**D**) Distance between ILC2s and lung stromal cells in steady state (Steady), papain-induced airway inflammation (Papain), and HDM-induced airway inflammation (HDM). (**E**) Heatmap of reanalyzed data on differentially expressed genes in bronchoalveolar lavage fluid ILC2s between acute (IL-33-induced) and chronic (HDM-induced) airway inflammation. (**F**) qRT-PCR analysis of *Ccr2* and *Ccr4* expression in ILC2s. (**G**) Mean fluorescence intensity (MFI) of CCR2 and CCR4 expression on ILC2s in steady state, papain-induced airway inflammation, and HDM-induced airway inflammation (n = 4). Data points were taken from more than three mice, with more than 20 cells of each type analyzed per mouse (C, D). Data are mean ± SEM with one-way ANOVA (C, D, F, G) and pooled from 2-3 independent experiments (C, D, F, G). *$p < 0.05$, **$p < 0.01$, ***$p < 0.001$, ****$p < 0.0001$.

Supplementary Figure 3. Anti-CCL17 antibody treatment diminishes the tendency of ILC2s to distribute near bronchi during papain-induced airway inflammation.
IL-5-Venus reporter mice treated with or without an anti-CCL17 antibody were subjected to papain-induced airway inflammation. (**A**) Absolute numbers of ILC2s, T cells, alveolar macrophages, monocytes, neutrophils, B cells, eosinophils, and NK cells in the lung parenchyma of IL-5$^{Venus/+}$ mice and control mice (n = 3-5). (**B**) Frequency of Venus$^+$ ILC2s of total ILC2s and mean fluorescence intensity (MFI) of Venus expression of ILC2s (n = 6). (**C**) MFI of ST2 expression of ILC2s (n = 6). (**D**) Absolute numbers of eosinophils and alveolar macrophages (AM) in the BALF (n = 5). (**E**) Distance between ILC2s and lung stromal cells in control or CCL17 Ab-treated mice. (**F**) Lung tissue samples (30 μm thickness) from IL-5$^{Venus/+}$ mice were stained with anti-EpCAM (yellow, bronchial structure), anti-Lyve1 (green, lymphatic vessels), anti-GFP (red, IL-5$^+$ ILC2s), and anti-CD3 (blue, T cells) antibodies. Images are representative of three or more mice. Scale bar, 100 μm. Data points were taken from mice with more than three animals with more than 20 cells of each type analyzed per mouse (E). Data are mean ± SEM with Student's *t*-test and pooled from 2-3 independent experiments (A-E). *$p < 0.05$, **$p < 0.01$, ***$p < 0.001$.

Supplementary Figure 4. Anti-CCL2 antibody treatment diminishes the tendency of ILC2s to distribute near lymphatic vessels in HDM-induced airway inflammation.
IL-5-Venus reporter mice treated with or without an anti-CCL2 antibody were subjected to HDM-induced airway inflammation. (**A**) Absolute numbers of ILC2s, T cells, alveolar macrophages, neutrophils, B cells, eosinophils, and NK cells in the lung parenchyma of IL-

$5^{Venus/+}$ mice and control mice (n = 4). (**B**) Frequency of $Venus^+$ ILC2s of total ILC2s and mean fluorescence intensity (MFI) of Venus expression of ILC2s (n = 3). (**C**) Frequency of $Venus^+$ T cells of total T cells and MFI of Venus expression of T cells (n = 3). (**D**) Absolute numbers of eosinophils and alveolar macrophages (AM) in the BALF (n = 3). (**E**) Distance between ILC2s and lung stromal cells in control or CCL2 Ab-treated mice. (**F**) Lung tissue samples (30 μm thickness) from IL-$5^{Venus/+}$ mice were stained with anti-EpCAM (yellow, bronchial structure), anti-Lyve1 (green, lymphatic vessels), anti-GFP (red, IL-5^+ ILC2s), and anti-CD3 (blue, T cells) antibodies. Images are representative for three or more mice. Scale bar, 100 μm. Data points were taken from mice with more than three animals with more than 20 cells of each type analyzed per mouse (E). Data are mean ± SEM with Student's *t*-test and pooled from 2−3 independent experiments (A-E). *$p < 0.05$, **$p < 0.01$, ****$p < 0.0001$.

Supplementary Figure 5. The numbers of lung immune cells in steady state are unchanged in the lung of IL-7cKO mice.
(**A**) Absolute numbers of T cells, B cells, NK cells, alveolar macrophages (AM), eosinophils, neutrophils, and dendritic cells (DC) in lung parenchyma from SPC-Cre IL-7cKO and control mice (n = 2-5). (**B**) Absolute numbers of T cells, B cells, NK cells, alveolar macrophages (AM), eosinophils, neutrophils, and dendritic cells (DC) in the lung from Lyve1-Cre IL-7cKO mice or control mice (n = 6). (**C**) Lung tissue samples (30 μm thickness) from control and SPC-Cre IL-7cKO mice (top) and control and Lyve1-Cre IL-7cKO mice (bottom) in steady state were stained with anti-EpCAM (yellow), anti-Lyve1 (green), anti-NKp46 (yellow), anti-CD25 (red), and anti-CD3 (blue, T cells) antibodies. ILC2s were identified as $CD3^-CD25^+NKp46^-$ round cells. Pictures are representative of three or more mice. Scale bar, 50 μm. Data are mean ± SEM with Student's *t*-test and pooled from 2-3 independent experiments (A, B).

Supplementary Figure 6. Lung immune cells are unchanged in IL-7cKO mice in papain-induced airway inflammation.
Papain-induced airway inflammation was performed as shown in Fig. 2A. (**A**) Flow cytometric analysis of Venus expression in parenchymal cells of IL-$5^{Venus/+}$ mice (n = 3). (**B**) Absolute numbers of total cells, T cells, B cells, NK cells, iNKT cells, alveolar macrophages (AM), eosinophils, neutrophils, ILC2s, and dendritic cells (DC) in lung parenchyma of control and SPC-Cre IL-7cKO mice (n = 3-4). (**C**) Absolute numbers of lung immune cells in control and Lyve1-Cre IL-7cKO mice (n = 4-5). (**D**) Mean fluorescence intensity (MFI) of IL-5 and IL-13 expression in ILC2s of control and SPC-Cre IL-7cKO mice (n = 3). (**E**) MFI of IL-5 and IL-13 expression in ILC2s of control and Lyve1-Cre IL-7cKO mice (n = 6). Data are mean ± SEM with Student's *t*-test and pooled from 2-3 independent experiments (B-E).

Supplementary Figure 7. Effect of IL-7 on the function of lung ILC2s.
(**A**, **B**) Histological images of representative lung sections of 10 μm thickness stained with H&E in control and SPC-Cre IL-7cKO mice (A) and in control and Lyve1-Cre IL-7cKO mice (B) by low power field (×4). (**C**) Lung ILC2s ($Lineage^-IL\text{-}7R^+CD25^+Sca\text{-}1^+$, 5×10^3/well) from wild-type mice were cultured with the indicated cytokines for three days. IL-5 and IL-13 in culture supernatants were measured by ELISA (n = 4-5). (**D**) Lung tissue samples (30 μm thickness) from control and SPC-Cre IL-7cKO mice (top) and control and Lyve1-Cre IL-7cKO mice (bottom) in papain-induced airway inflammation were stained with anti-EpCAM (yellow), anti-Lyve1 (green), anti-NKp46 (yellow), anti-CD25 (red), and anti-CD3 (blue, T cells) antibodies. ILC2s were identified as $CD3^-CD25^+NKp46^-$ round cells. Pictures are representative of three or more mice. Scale bar, 50 μm. Data are mean ± SEM with one-way ANOVA and pooled from 2-3 independent experiments (C)*$p < 0.05$, **$p < 0.01$, ***$p < 0.001$, ****$p < 0.0001$.

Supplementary Figure 8. Lung immune cells are unchanged in IL-7cKO mice in HDM-induced airway inflammation.
HDM-induced airway inflammation was performed as shown in Fig. 2B. (**A**) Absolute numbers of lung immune cells in control and SPC-Cre IL-7cKO mice (n = 4-5). (**B**) Absolute numbers of lung immune cells in control and Lyve1-Cre IL-7cKO mice (n = 5-6). (**C**) Mean fluorescence intensity (MFI) of Bcl-2 and Ki-67 expression in ILC2s of control and SPC-Cre IL-7cKO mice (n = 3). (**D**) MFI of IL-5 and IL-13 expression in ILC2s of control and SPC-Cre IL-7cKO mice (n = 3). (**E**) MFI of IL-5 and IL-13 expression in ILC2s of control and Lyve1-Cre IL-7cKO mice (n = 4). (**F**) Lung tissue samples (30 μm thickness) from control and SPC-Cre IL-7cKO mice (top) and control and Lyve1-Cre IL-7cKO mice (bottom) in HDM-induced airway inflammation were stained with anti-EpCAM (yellow), anti-Lyve1 (green), anti-NKp46 (yellow), anti-CD25 (red), and anti-CD3 (blue, T cells) antibodies. ILC2s were identified as $CD3^{-}CD25^{+}NKp46^{-}$ round cells. Pictures are representative of three or more mice. Scale bar, 50 μm. Data are mean ± SEM with Student's *t*-test and pooled from 2-3 independent experiments (A-E).

Supplementary Figure 9. Histological images of IL-7cKO mice in HDM-induced airway inflammation.
HDM-induced airway inflammation was performed as shown in Fig. 2B. (A-D) Histological images of representative lung sections of 10 μm thickness stained with H&E in control and SPC-Cre IL-7cKO mice (A, B) and in control and Lyve1-Cre IL-7cKO mice (C, D) by high-power field (×20) (A, C) and low-power field (×4) (B, D) (n =3).

Supplementary Figure 10. IL-7 expression in stromal cells is unchanged between steady state and inflammation.
GFP expression in stromal cells of $IL\text{-}7^{GFP/+}$ mice in papain- and HDM-induced airway inflammation. Data represent two independent experiments with similar results (n = 3).

Supplementary Figure 11. Flow cytometric analysis of lung immune cells in anti-IL-7 antibody-treated or control mice.
Absolute numbers of lung immune cells in control and anti-IL-7 antibody-treated mice (n = 2-12). Alleviation of papain-induced airway inflammation by the anti-IL-7 antibody was performed as shown in Fig. 6A. Data are mean ± SEM with Student's *t*-test.

Figure 1

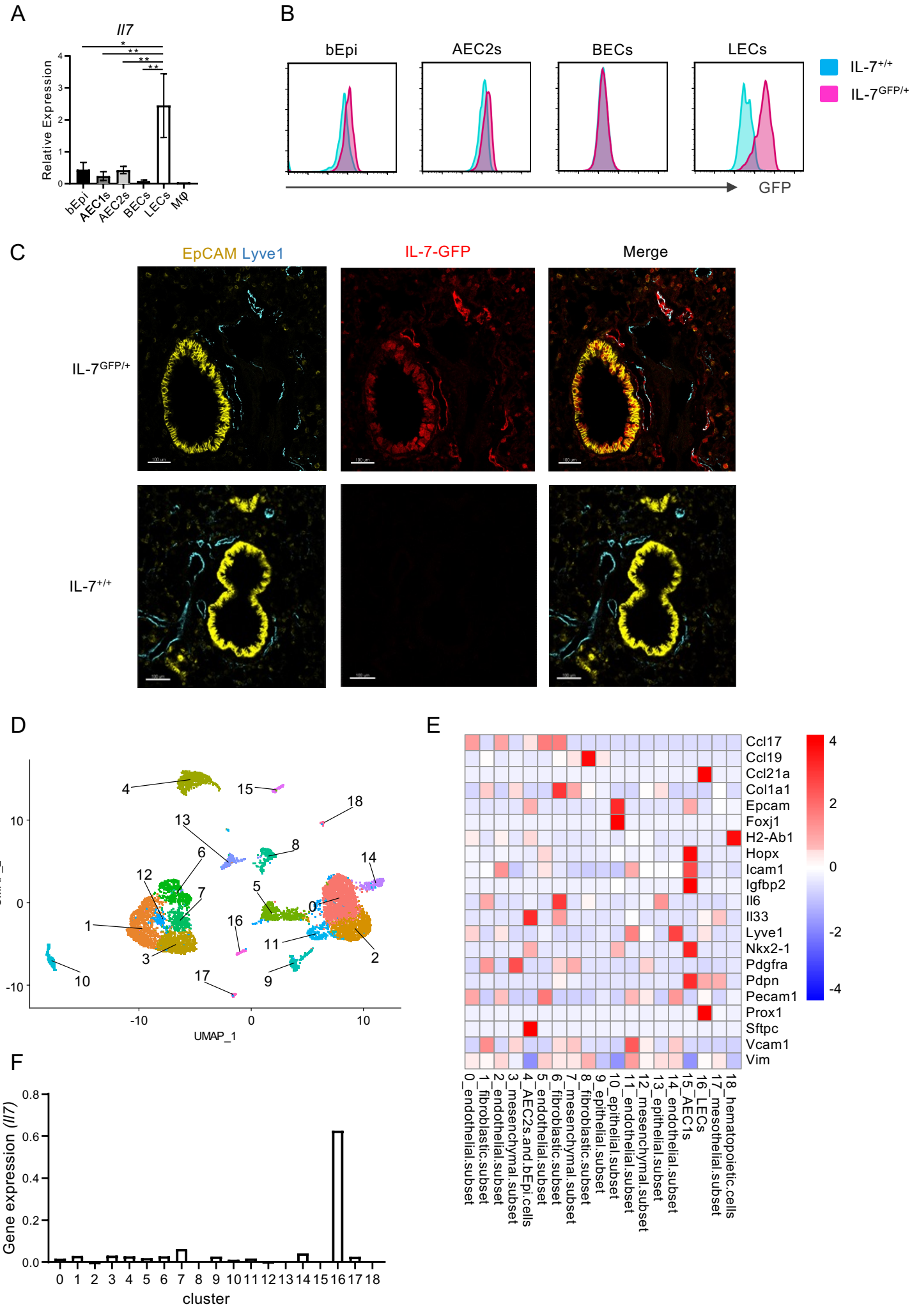
A
Il7
Relative Expression
bEpi
AEC1s
AEC2s
BECs
LECs
Mφ
B
bEpi
AEC2s
BECs
LECs
IL-7+/+
IL-7GFP/+
GFP
C
EpCAM Lyve1
IL-7-GFP
Merge
IL-7GFP/+
IL-7+/+
D
UMAP_2
UMAP_1
E
Ccl17
Ccl19
Ccl21a
Col1a1
Epcam
Foxj1
H2-Ab1
Hopx
Icam1
Igfbp2
Il6
Il33
Lyve1
Nkx2-1
Pdgfra
Pdpn
Pecam1
Prox1
Sftpc
Vcam1
Vim
0_endothelial.subset
1_fibroblastic.subset
2_endothelial.subset
3_mesenchymal.subset
4_AEC2s.and.bEpi.cells
5_endothelial.subset
6_fibroblastic.subset
7_mesenchymal.subset
8_fibroblastic.subset
9_epithelial.subset
10_epithelial.subset
11_endothelial.subset
12_mesenchymal.subset
13_epithelial.subset
14_endothelial.subset
15_AEC1s
16_LECs
17_mesothelial.subset
18_hematopoietic.cells
F
Gene expression (Il7)
cluster

Figure 2

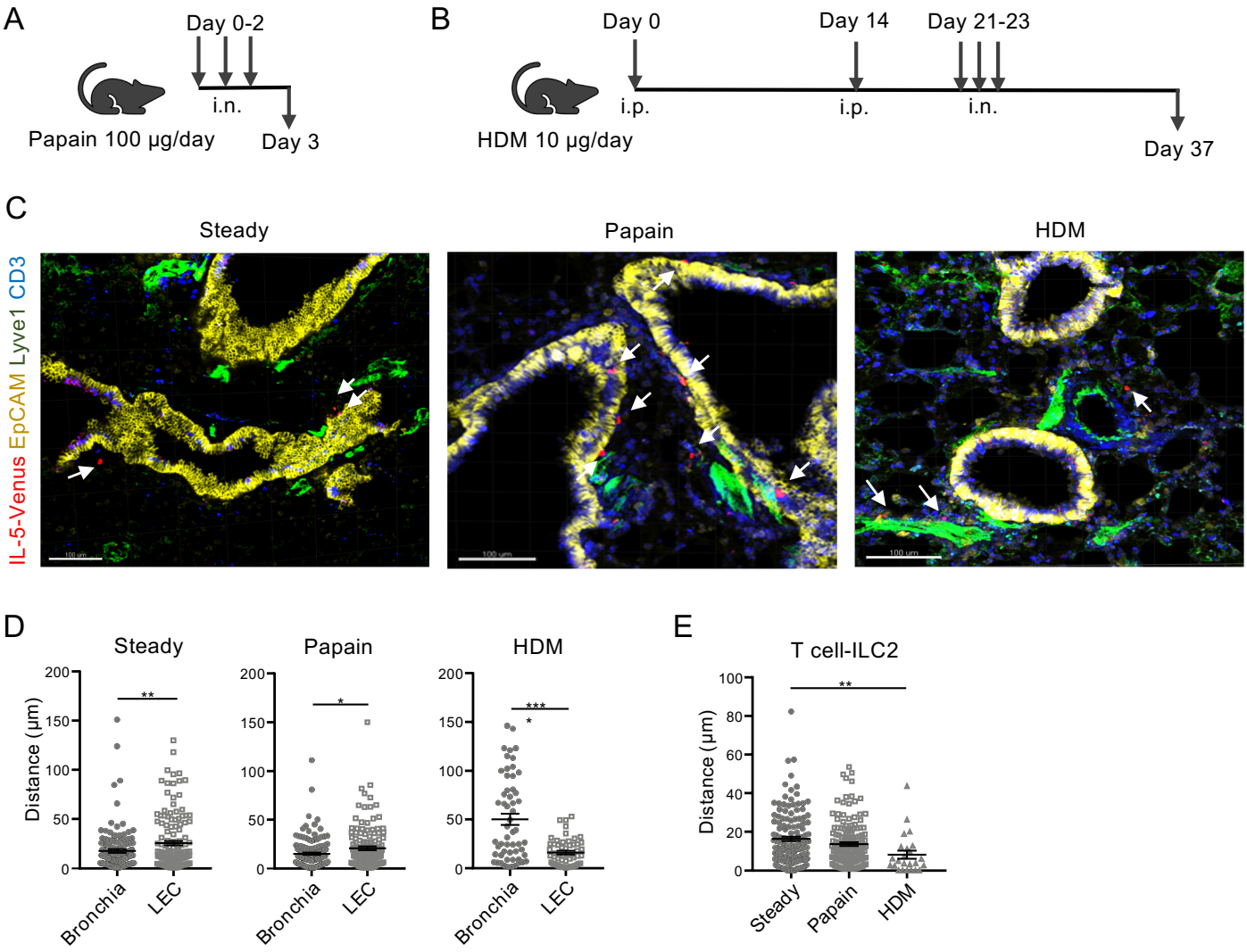
A
Day 0-2
i.n.
Papain 100 µg/day
Day 3
B
Day 0
Day 14
Day 21-23
i.p.
i.p.
i.n.
HDM 10 µg/day
Day 37
C
Steady
Papain
HDM
IL-5-Venus EpCAM Lyve1 CD3
D
Steady
Papain
HDM
Distance (µm)
Bronchia
LEC
E
T cell-ILC2
Distance (µm)
Steady
Papain
HDM

Figure 3

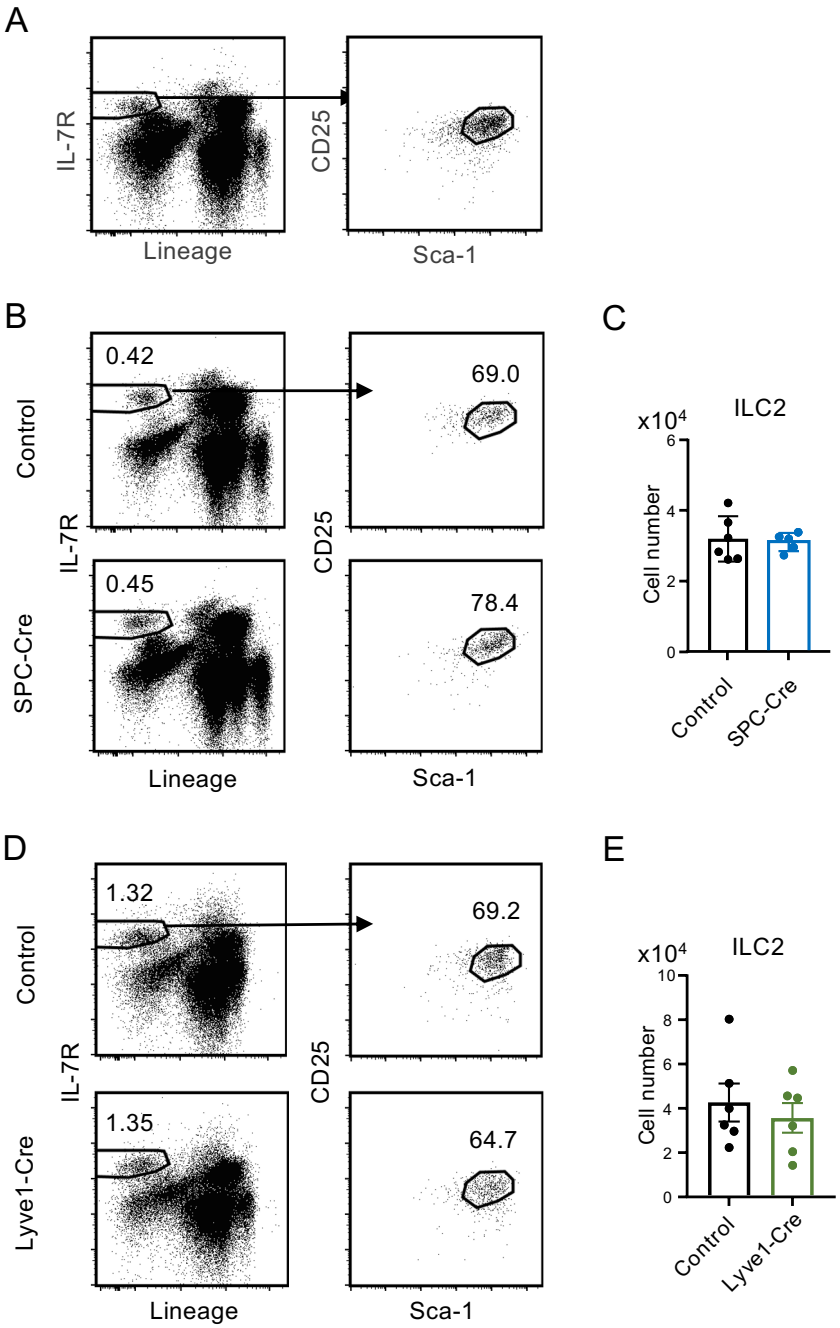
A
IL-7R
Lineage
CD25
Sca-1
B
Control
SPC-Cre
0.42
69.0
0.45
78.4
IL-7R
CD25
Lineage
Sca-1
C
ILC2
x10⁴
Cell number
Control
SPC-Cre
D
Control
Lyve1-Cre
1.32
69.2
1.35
64.7
IL-7R
CD25
Lineage
Sca-1
E
ILC2
x10⁴
Cell number
Control
Lyve1-Cre

Figure 4

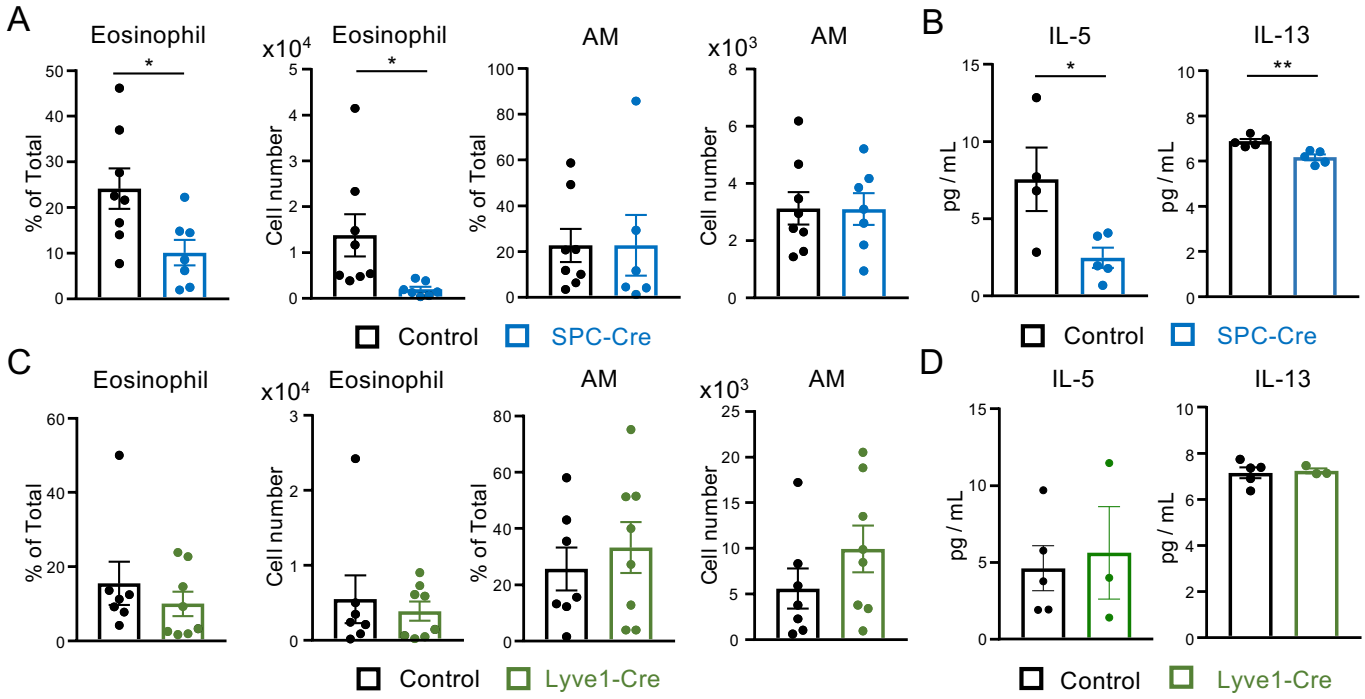
A
Eosinophil
% of Total
Eosinophil
x10^4
Cell number
AM
% of Total
AM
x10^3
Cell number
Control
SPC-Cre
B
IL-5
pg / mL
IL-13
pg / mL
Control
SPC-Cre
C
Eosinophil
% of Total
Eosinophil
x10^4
Cell number
AM
% of Total
AM
x10^3
Cell number
Control
Lyve1-Cre
D
IL-5
pg / mL
IL-13
pg / mL
Control
Lyve1-Cre

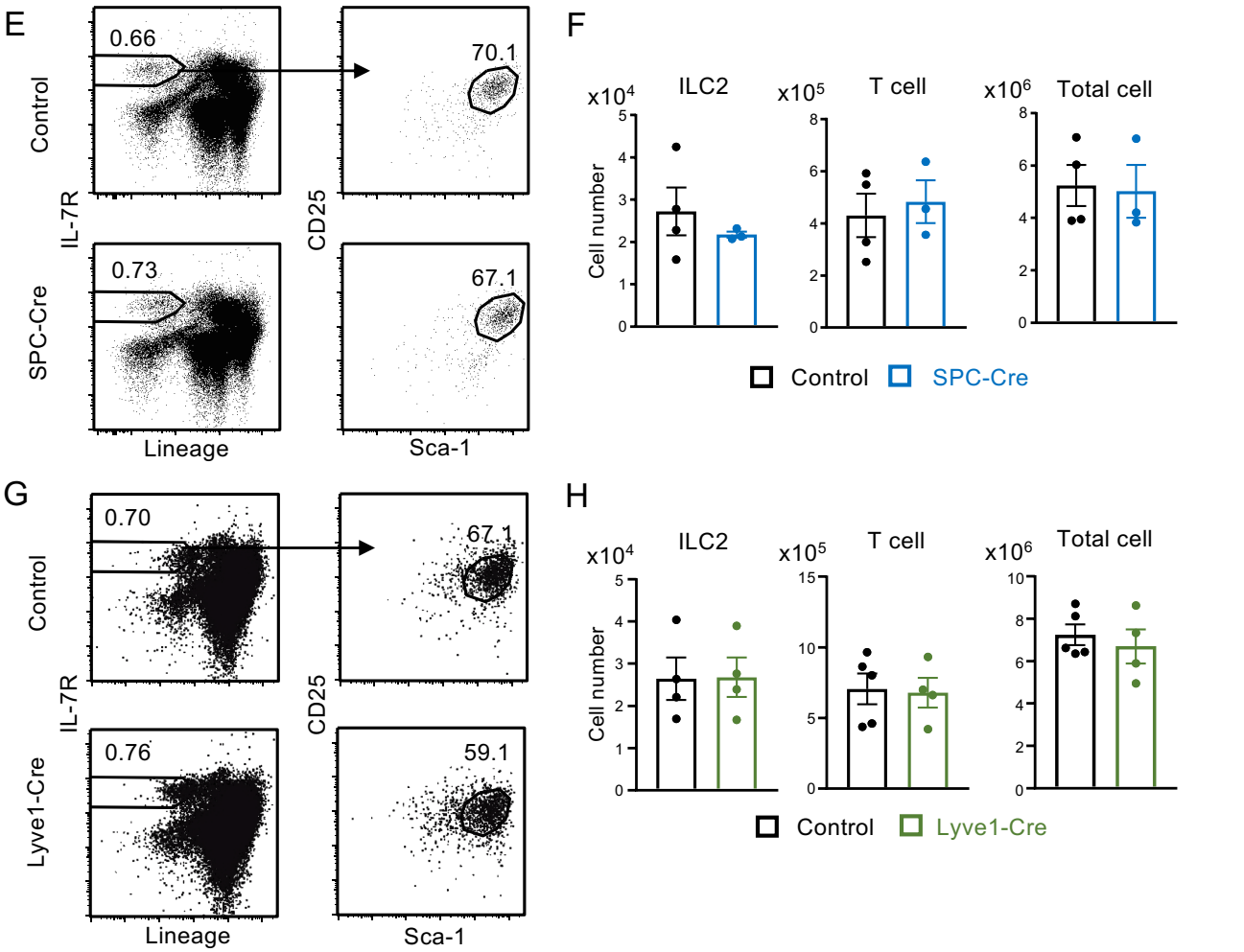
E
0.66
70.1
Control
IL-7R
CD25
0.73
67.1
SPC-Cre
Lineage
Sca-1
F
ILC2
x10^4
T cell
x10^5
Total cell
x10^6
Cell number
Control
SPC-Cre
G
0.70
67.1
Control
IL-7R
CD25
0.76
59.1
Lyve1-Cre
Lineage
Sca-1
H
ILC2
x10^4
T cell
x10^5
Total cell
x10^6
Cell number
Control
Lyve1-Cre

Figure 5

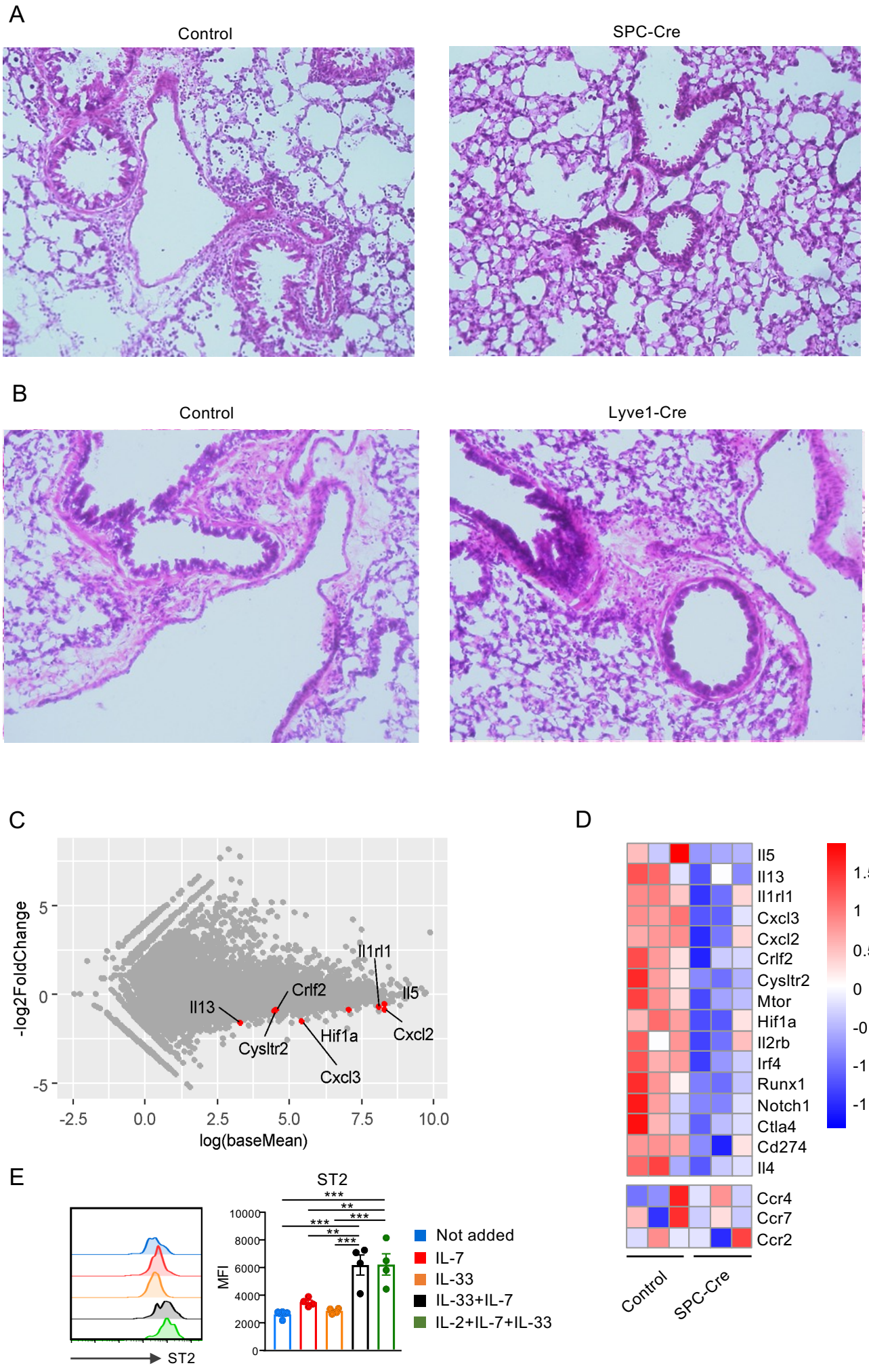
A
Control
SPC-Cre
B
Control
Lyve1-Cre
C
-log2FoldChange
log(baseMean)
Il1rl1
Crlf2
Il5
Il13
Hif1a
Cysltr2
Cxcl2
Cxcl3
D
Il5
Il13
Il1rl1
Cxcl3
Cxcl2
Crlf2
Cysltr2
Mtor
Hif1a
Il2rb
Irf4
Runx1
Notch1
Ctla4
Cd274
Il4
Ccr4
Ccr7
Ccr2
Control
SPC-Cre
E
ST2
MFI
Not added
IL-7
IL-33
IL-33+IL-7
IL-2+IL-7+IL-33

Figure 6

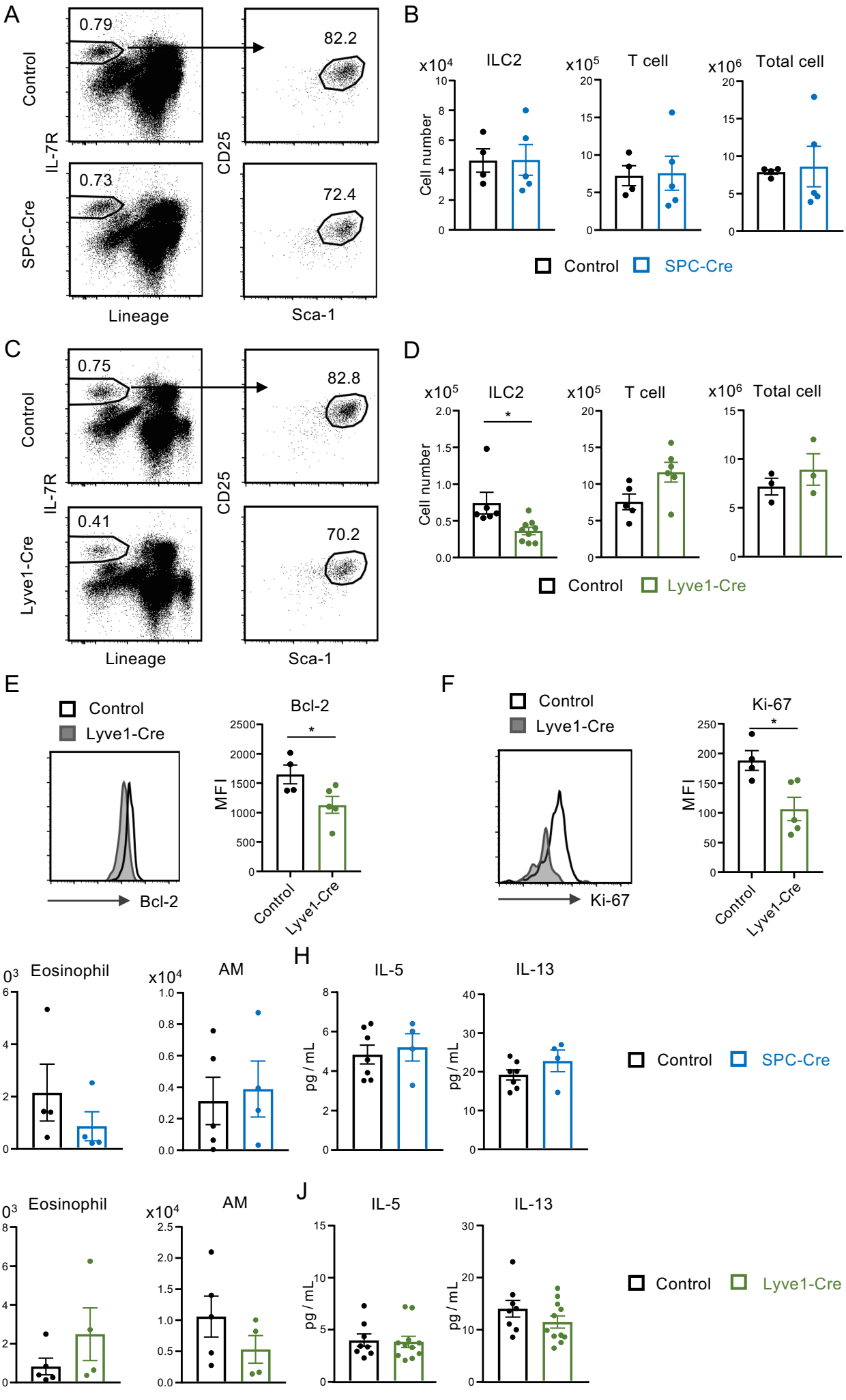
A
0.79
82.2
Control
IL-7R
CD25
0.73
72.4
SPC-Cre
Lineage
Sca-1
B
x10⁴ ILC2
x10⁵ T cell
x10⁶ Total cell
Cell number
Control
SPC-Cre
C
0.75
82.8
Control
IL-7R
CD25
0.41
70.2
Lyve1-Cre
Lineage
Sca-1
D
x10⁵ ILC2
x10⁵ T cell
x10⁶ Total cell
Cell number
*
Control
Lyve1-Cre
E
Control
Lyve1-Cre
Bcl-2
MFI
*
Control
Lyve1-Cre
F
Control
Lyve1-Cre
Ki-67
MFI
*
Control
Lyve1-Cre
G
x10³ Eosinophil
x10⁴ AM
Cell number
H
IL-5
IL-13
pg / mL
Control
SPC-Cre
I
x10³ Eosinophil
x10⁴ AM
Cell number
J
IL-5
IL-13
pg / mL
Control
Lyve1-Cre

Figure 7

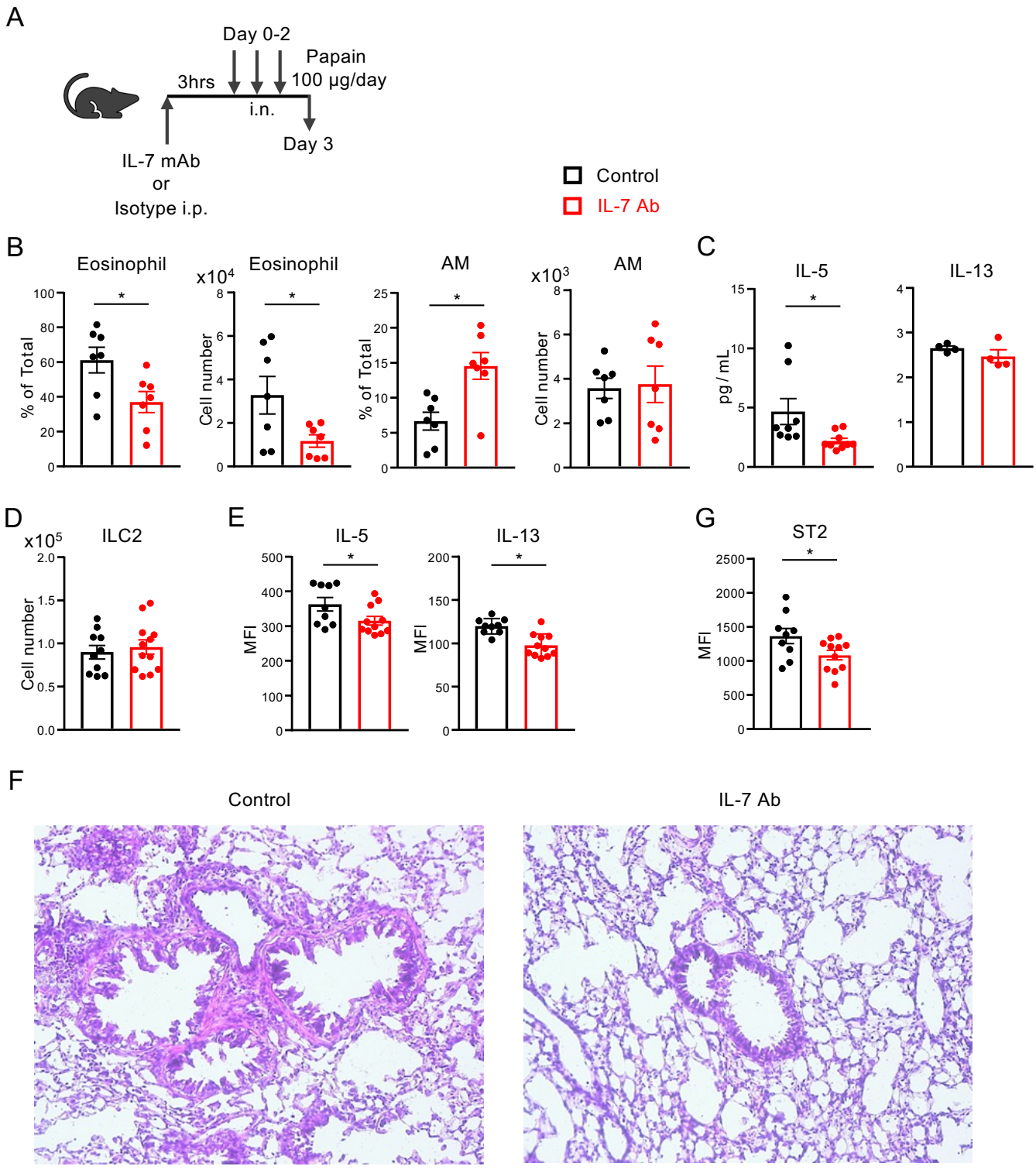
A
Day 0-2
Papain
100 µg/day
3hrs
i.n.
Day 3
IL-7 mAb
or
Isotype i.p.
Control
IL-7 Ab
B
Eosinophil
% of Total
Eosinophil
x10^4
Cell number
AM
% of Total
AM
x10^3
Cell number
C
IL-5
pg / mL
IL-13
D
ILC2
x10^5
Cell number
E
IL-5
MFI
IL-13
MFI
G
ST2
MFI
F
Control
IL-7 Ab

Supplementary Figure 1

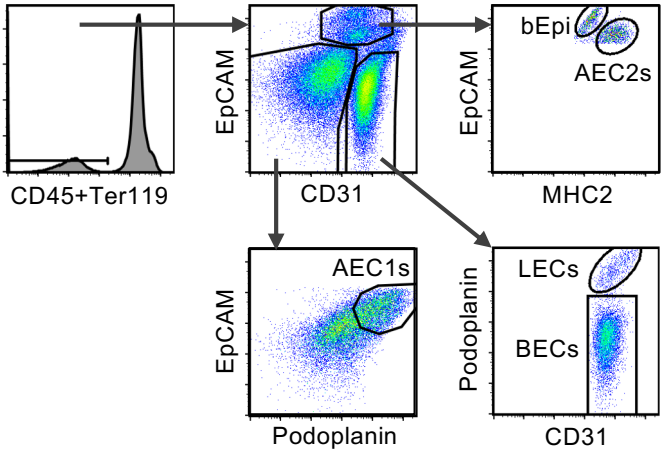

Supplementary Figure 2

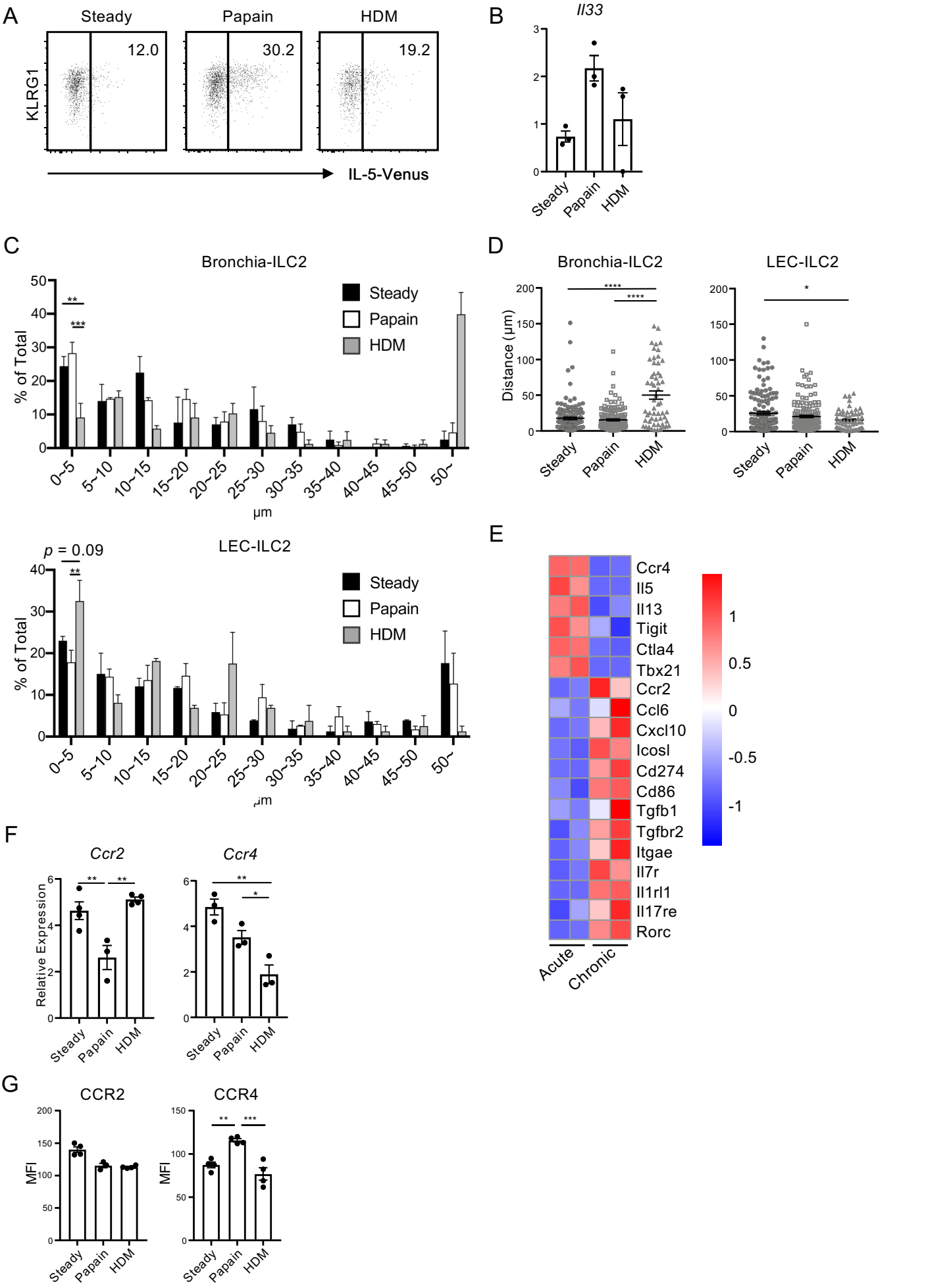

Supplementary Figure 3

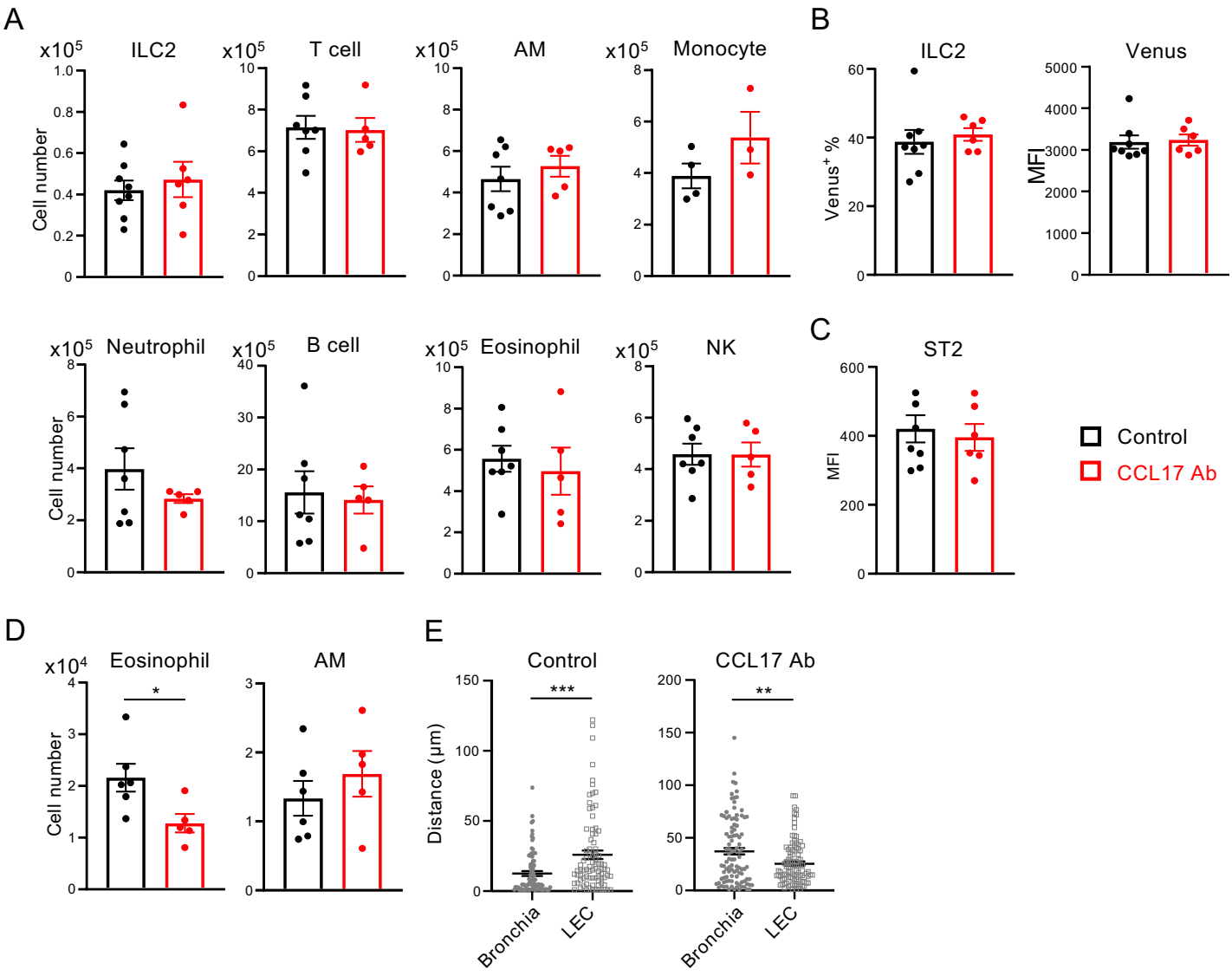

Supplementary Figure 4

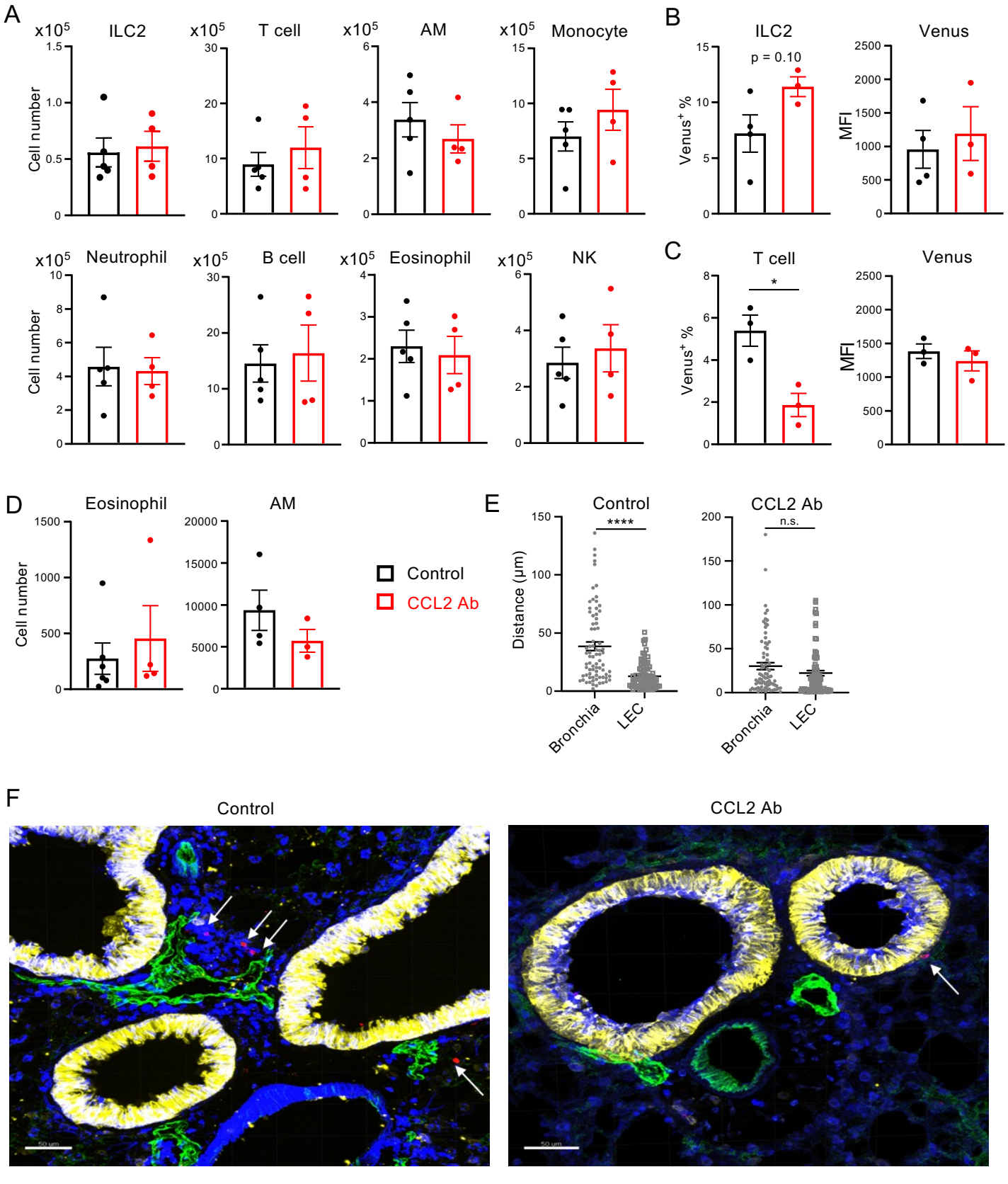

Supplementary Figure 5

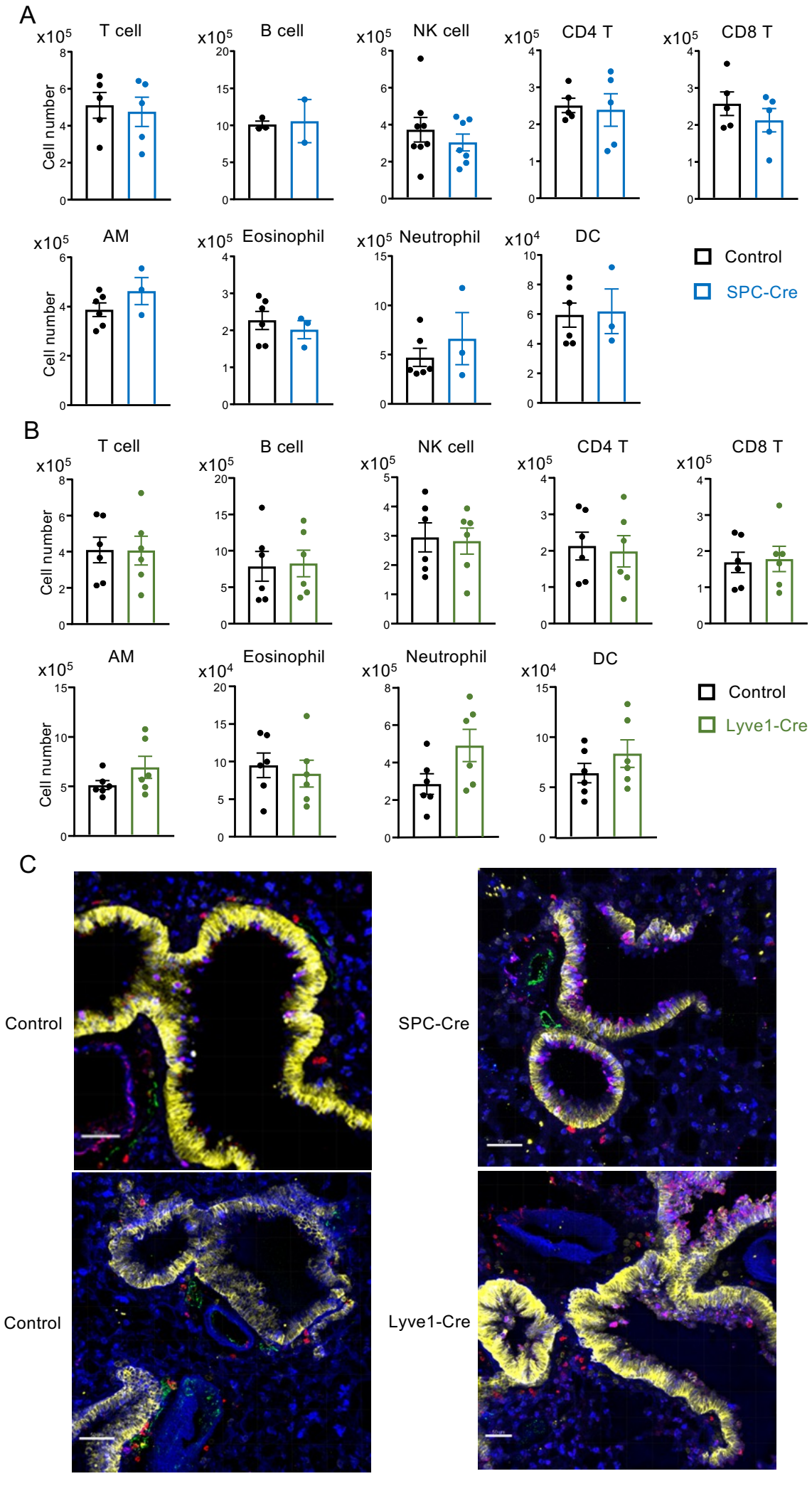

Supplementary Figure 6

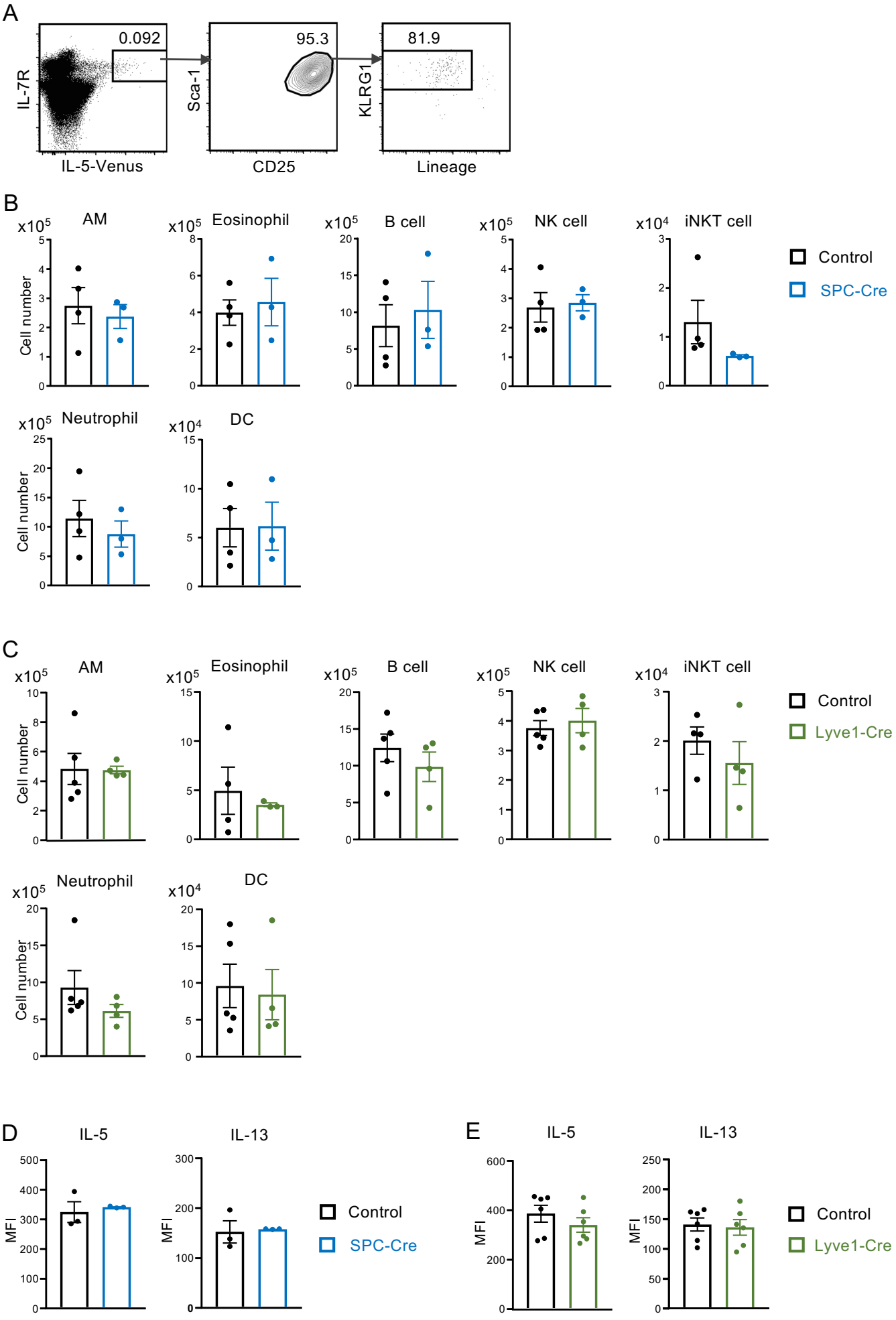

Supplementary Figure 7

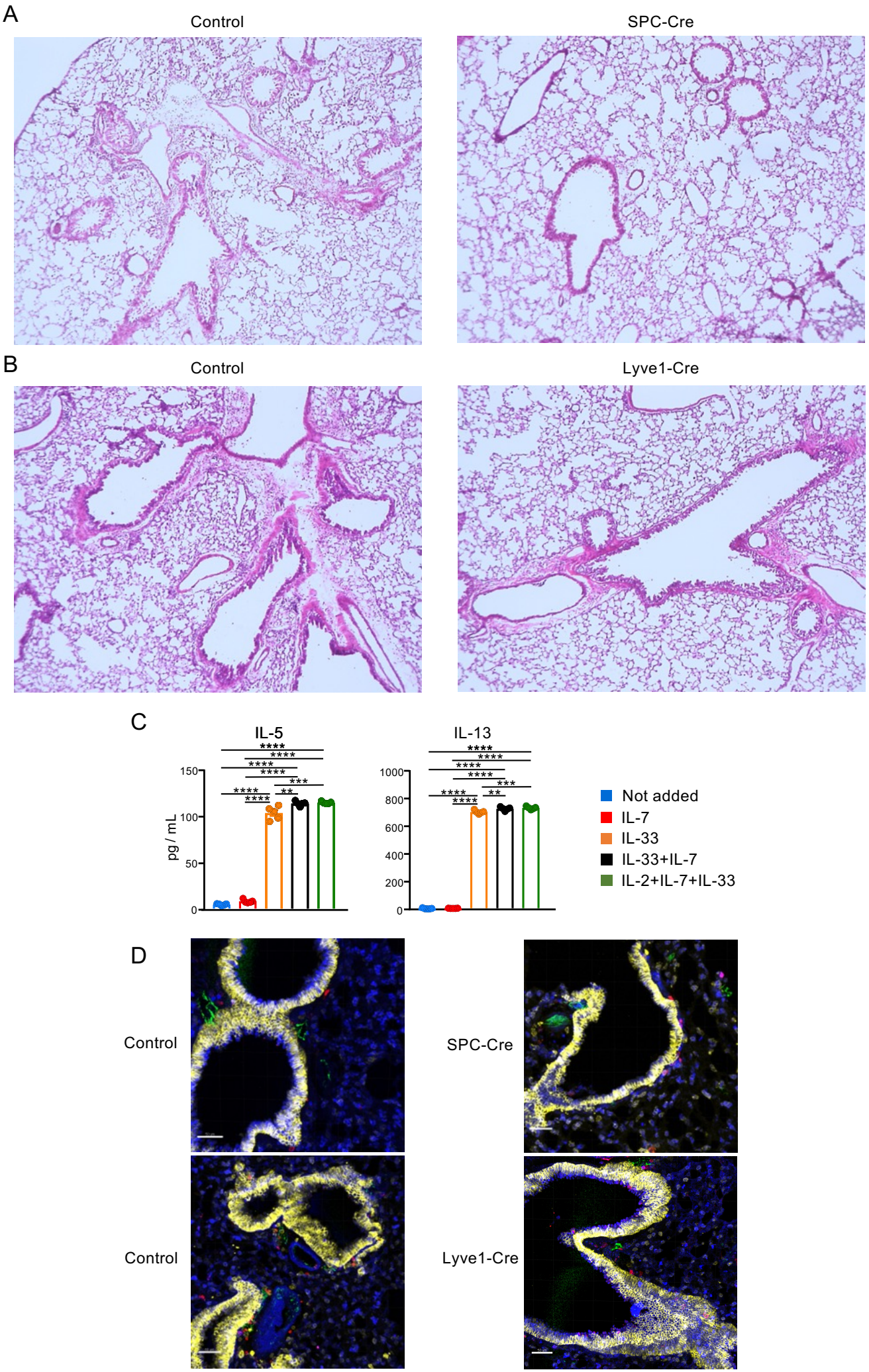

Supplementary Figure 8

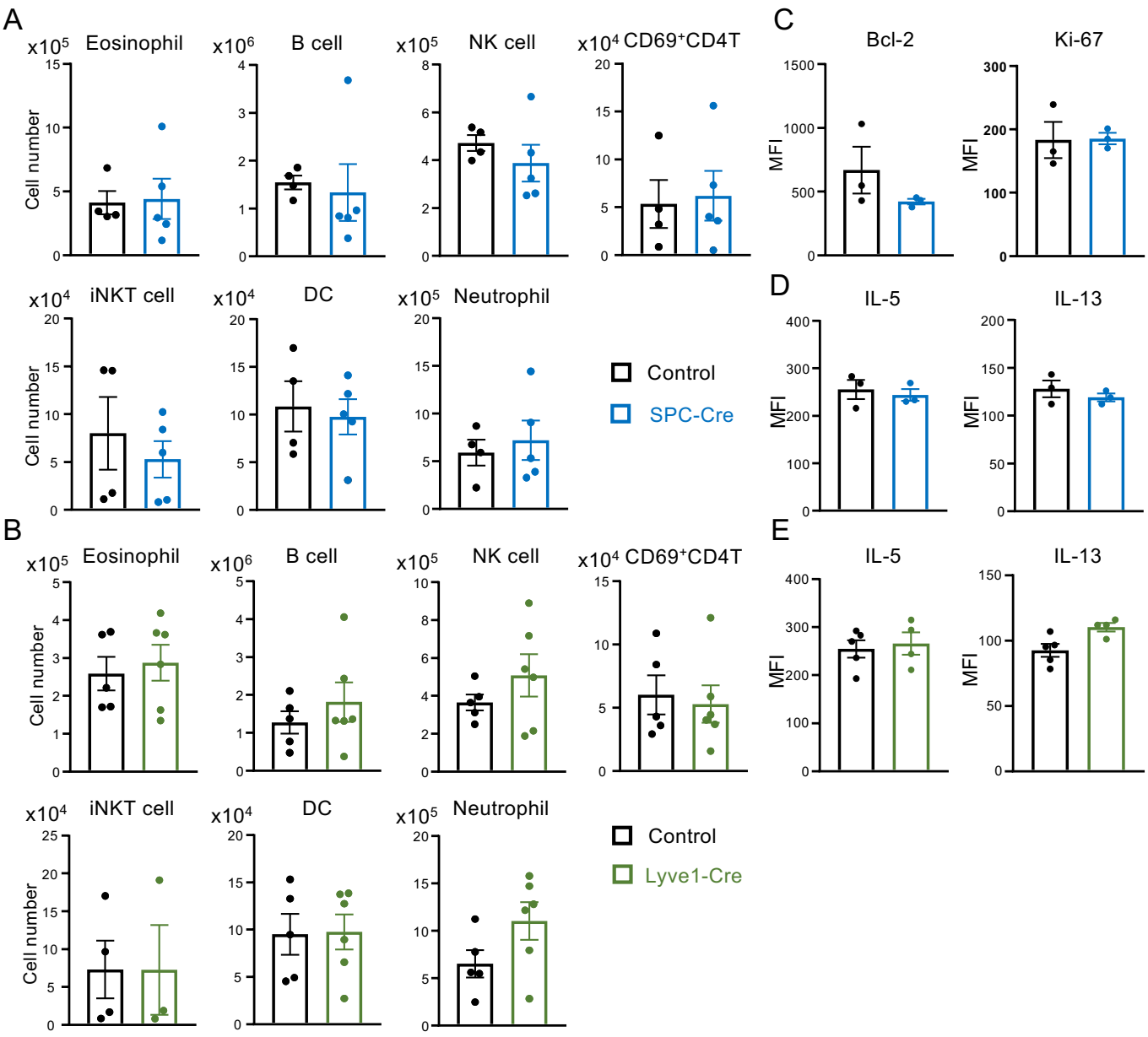

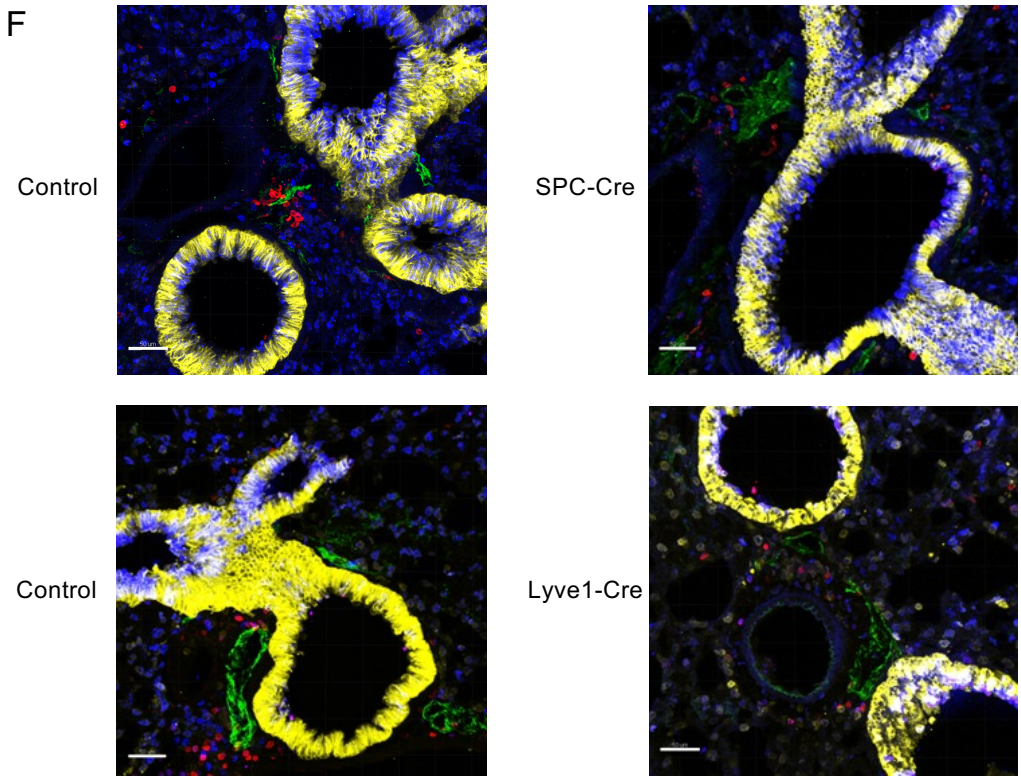

Supplementary Figure 9

A

Control

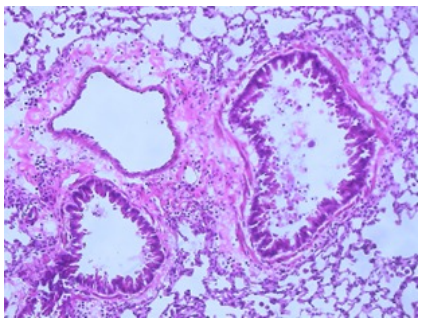

SPC-Cre

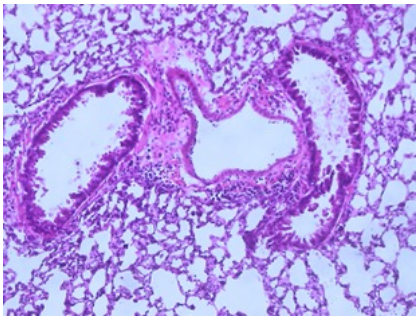

B

Control

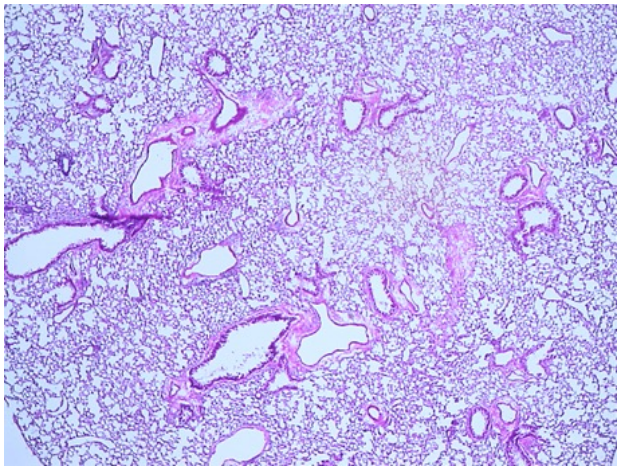

SPC-Cre

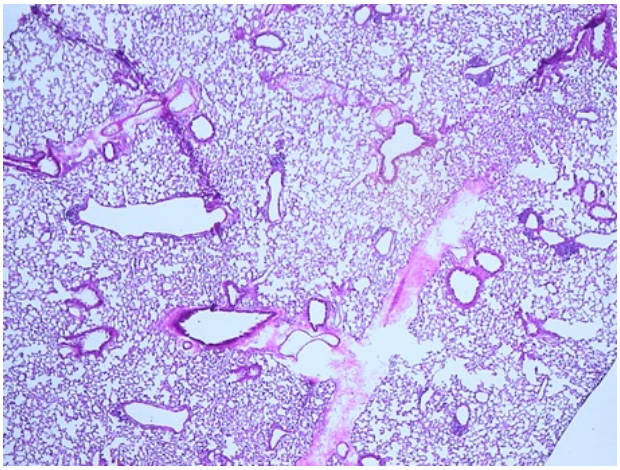

C

Control

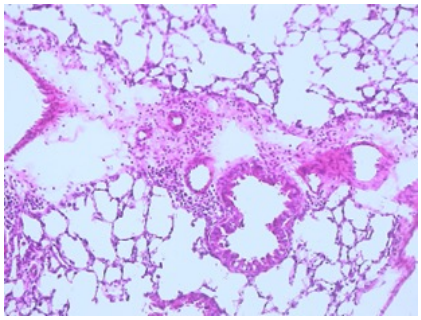

Lyve1-Cre

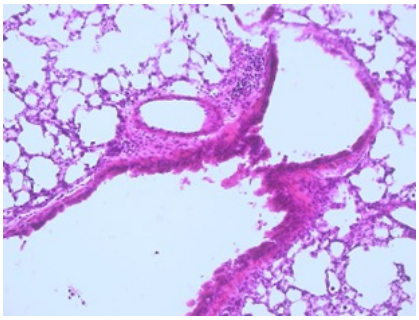

D

Control

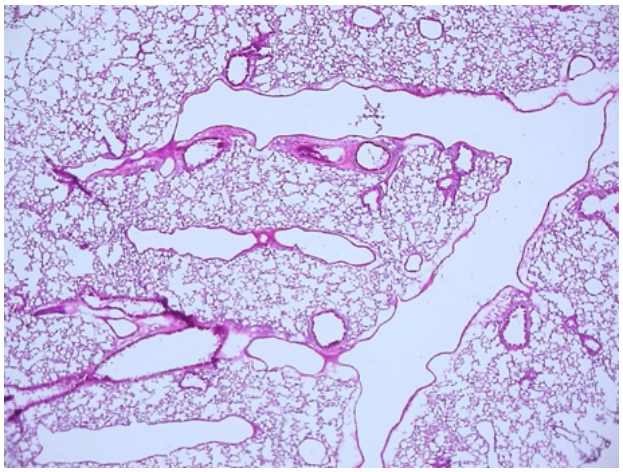

Lyve1-Cre

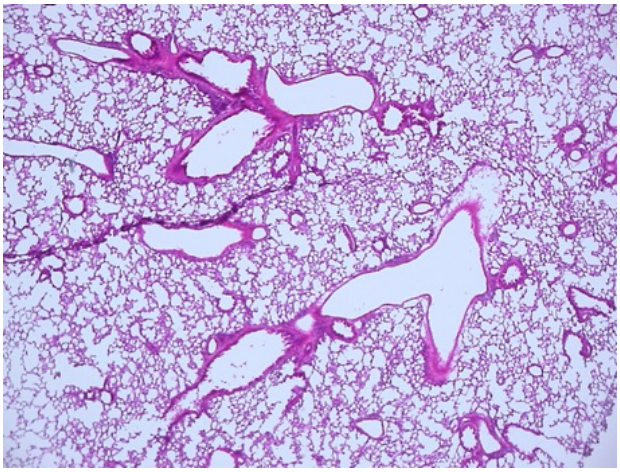

Supplementary Figure 10

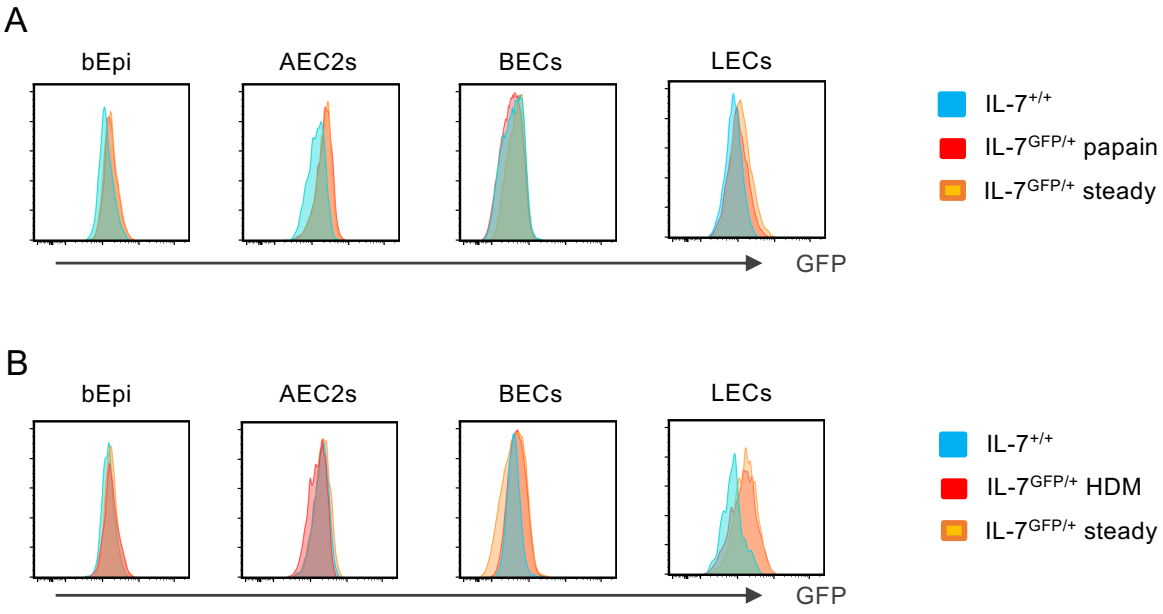

Supplementary Figure 11